Fast ATP-dependent subunit rotation in reconstituted F_oF_1-ATP synthase trapped in solution

Thomas Heitkamp, Michael Börsch [1]

Single-Molecule Microscopy Group, Jena University Hospital, D-07743 Jena, Germany.

KEYWORDS: single-molecule enzymology, F_oF_1-ATP synthase, ATP hydrolysis, subunit rotation, single-molecule FRET, ABEL trap.

ABSTRACT: F_oF_1-ATP synthases are the ubiquitous membrane enzymes which catalyze ATP synthesis or ATP hydrolysis in reverse, respectively. Enzyme kinetics are controlled by internal subunit rotation, by substrate and product concentrations, by mechanical inhibitory mechanisms, but also by the electrochemical potential of protons across the membrane. By utilizing an Anti-Brownian electrokinetic trap (ABEL trap), single-molecule Förster resonance energy transfer (smFRET)-based subunit rotation monitoring was prolonged from milliseconds to seconds. The extended observation times for single proteoliposomes in solution allowed to observe fluctuating rotation rates of individual enzymes and to map the broad distributions of ATP-dependent catalytic rates in F_oF_1-ATP synthase. The buildup of an electrochemical potential of protons was confirmed to limit the maximum rate of ATP hydrolysis. In the presence of ionophores and uncouplers the fastest subunit rotation speeds measured in single reconstituted F_oF_1-ATP synthases were 180 full rounds per second, i.e. much faster than measured by biochemical ensemble averaging, but not as fast as the maximum rotational speed reported previously for isolated single F_1 fragments without coupling to the membrane-embedded F_o domain of the enzyme.

1. INTRODUCTION

[1] Corresponding author: michael.boersch@med.uni-jena.de

Enzymes are proteins that catalyze a comprehensive diversity of chemical reactions, for example redox reactions, cleavage or formation of chemical bonds or transfer of functional groups. Catalysis is associated with small or large conformational changes of the enzyme during the processes of binding the substrate molecules or releasing the products. The speed of catalysis covers a huge range of substrate turnover numbers, from 10^7 s^{-1} for the enzyme catalase [1] to 3000 s^{-1} for urease [2] to 2 s^{-1} for the two-step reaction of tryptophan synthase [3]. Kinetics of soluble enzymes in isotropic environments depend on the concentration of substrate molecules, on temperature, on buffer conditions and on the presence of activating or inhibitory small molecules including the products of the catalytic reaction. In addition, turnover of enzymes which are embedded in lipid membranes is affected by the lipids, by the membrane fluidity and curvature, by an electric membrane potential and by the asymmetry of concentrations of ions and molecules on both sides of the lipid bilayer.

F_oF_1-ATP synthases are membrane enzymes which catalyze the synthesis of adenosine triphosphate (ATP) in living cells. They are localized in the plasma membrane of bacteria, in the thylakoid membranes in chloroplasts of plant cells and in the inner mitochondrial membrane of eukaryotic cells. For F_oF_1-ATP synthase from *Escherichia coli*, the electric membrane potential $\Delta\psi$ complements the difference of proton concentrations ΔpH across the plasma membrane as the driving force for ATP formation [4, 5]. i.e. this proton motive force (*pmf*) comprises ΔpH and $\Delta\psi$. Maximum ATP synthesis rates at very high *pmf* were determined between 100 ATP·s^{-1} for purified enzymes reconstituted in artificial liposomes at 23°C [6] and 270 ATP·s^{-1} for membrane vesicles using the native lipid-protein composition at 37°C [7]. However, under realistic conditions with a smaller *pmf* and a physiological ATP/ADP ratio, ATP synthesis rates were significantly lower, i.e. in the range of 1 to 10 ATP·s^{-1} measured in native membrane vesicles [4b, 8, 9, 10].

F_oF_1-ATP synthases from *E. coli* also catalyze the reverse chemical reaction, i.e. the hydrolysis of ATP to ADP and phosphate. Catalytic turnover numbers for ATP hydrolysis at room temperature were reported in the range of 60 ATP·s^{-1} for reconstituted enzymes in a liposome [11], 145 ATP·s^{-1} for enzymes reconstituted in lipid nanodiscs [12], or 300 ATP·s^{-1} for enzymes solubilized in detergent micelles [5]. The different kinetics are due to the active pumping of protons across the lipid bilayer during ATP hydrolysis. Liposomes are closed vesicles, and pumping protons into the vesicle will create an increasing pH difference and generate an electric membrane potential, i.e. the buildup of a counteracting *pmf*. Accordingly, addition of protonophores or uncouplers to dissipate a ΔpH or

$\Delta\psi$ increases the maximum ATP hydrolysis rates of reconstituted F_oF_1-ATP synthases in liposomes by factors of 2 [13] to 5 [11], in good agreement to the rates of solubilized enzymes in detergent micelles.

To maintain the required physiological ATP/ADP ratio in living cells, catalysis of the ATP hydrolysis reaction by F_oF_1-ATP synthases is strictly controlled. Two types of independent inhibitory mechanisms have been identified. For the *E. coli* and other bacterial F_oF_1-ATP synthases, regulation of ATP hydrolysis is achieved either by a large conformational change of the C-terminal domain of the ε subunit (εCTD) in the F_1 part, i.e. ε inhibition, or by binding of ADP to one catalytic site in F_1, i.e. ADP inhibition. Truncation mutations of the εCTD resulted in threefold increased ATP hydrolysis rates of reconstituted F_oF_1-ATP synthase [5]. The *pmf* might affect the conversion of the inhibitory conformation of εCTD. For example, pre-energization of proteoliposomes with F_oF_1-ATP synthase, achieved by applying ΔpH and $\Delta\psi$, resulted in a short-term, up to ninefold increase of ATP hydrolysis rates in the presence of ADP and phosphate compared to proteoliposomes without a *pmf* [11]. Discriminating and quantifying these two control mechanisms are currently important experimental challenges, studied with both F_oF_1-ATP synthases and their respective F_1 fragments from various bacteria, including pathogens like *Mycobacterium tuberculosis* [14, 14b, 15].

Already more than 20 years ago, i.e. only a few years after the first demonstration of single dye detection in an organic host matrix at cryogenic temperatures [16], kinetics of individual enzymes were investigated. For soluble lactate dehydrogenase, catalytic activities were found to vary from enzyme to enzyme by a factor of four using the fluorescence intensity of the product molecules as the read-out [17]. Recording single-molecule fluorescence intensity traces of the endogenous chromophore FAD in cholesterol oxidase revealed fluctuations of catalytic rates between different enzyme molecules, but also stochastic fluctuations of turnover numbers within time traces of a single enzyme [18]. Compared to biochemical assays based on ensemble averaging, single-molecule enzymology promises to unravel sequence and timing of the individual catalytic steps, substeps and intermediates, the directionality of catalysis by monitoring forward and backward steps, i.e. to elucidate the *static disorder* and the *dynamic disorder* of these molecular machines [19]. However, carefully re-purifying enzyme batches to homogeneity revealed that apparently variable activities from enzyme to enzyme could be caused by a heterogeneity of the enzyme sample, for example

due to enzyme aggregation, posttranslational modification, or partial degradation as shown for single alkaline phosphatase kinetics [20, 20b].

At the same time more than 20 years ago, single-molecule Förster resonance energy transfer (smFRET) for monitoring the distance between two specifically attached fluorophores on a single biomolecule was emerging [21]. SmFRET enabled a new focus on the conformational changes of enzymes associated with catalysis (for a recent smFRET review see [22]). Thereby, the need of using fluorescent substrates or products can be overcome, i.e. limitations by using a very low substrate concentration in the nanomolar range, substrate derivatives with altered catalytic kinetics or a high fluorescent background are avoided.

SmFRET allows to study catalysis especially with enzymes which cannot be synchronized to a specific starting conformation of the catalytic cycle. For example, an enzyme runs through a unidirectional sequence of conformations →(1)→(2)→(3)→(1)→ and so on. Each conformation is identified and can be discriminated by smFRET due to the high precision of the distance measurement in the sub-nanometer (i.e. Å) range [23]. Then this sequential order of catalytic conformations can be unraveled observing one enzyme after another. Regardless of the first detected conformation (1), (2) or (3), respectively, in each individual enzyme, analyzing a set of time trajectories of smFRET-assigned conformations will provide the catalytic sequence. Dwell times and transition rates of these conformations can be determined. The probability of backwards steps or reversibility of the catalytic cycle might be identified, and the influence of substrate concentration, inhibitors and other parameters on turnover rates can be measured.

F_oF_1-ATP synthase is a non-synchronizable membrane enzyme due to its asymmetric structure. Its "*rotary mechanism*" for sequential catalysis on the three catalytic sites in the F_1 part was proposed by P. Boyer (see review [24]). First unequivocal evidence for this mechanism was achieved by x-ray crystallography structures of F_1 parts reported from J. Walker's group [25], followed by sophisticated biochemical [26] and spectroscopic experiments [27]. However, video-microscopy provided direct observation of the unidirectionally rotating central γ-subunit in a single F_1 fragment driven by ATP hydrolysis [28] and inaugurated single-molecule enzymology of the catalytic F_1 domain. This single-molecule approach, i.e. recording a light-scattering or a fluorescent marker on the rotating γ-subunit of F_1-ATPase attached to the cover glass on a microscope, revealed substrate-dependent kinetics

of the catalytic conformations, rotary substeps for substrate binding and product release, back steps, temperature dependence, inhibition by small molecules including ADP and by the εCTD (for reviews see [29, 30]), and enabled high-resolution computational analyses of rotary catalysis. Comparison of F_1 fragments from different species showed significant differences between the rotary substeps of the γ-subunit in bacterial and in mitochondrial F_1-ATPases [31, 32]. Single-molecule enzymology of the entire F_oF_1-ATP synthase could use the same approach for studying ATP hydrolysis, i.e. light-scattering or fluorescent markers on the rotating ring of c-subunits in the F_o part with the enzyme attached to the surface *via* the static subunits of the F_1 part, or *vice versa* [12, 33].

Alternatively, smFRET was established to analyze the rotary steps of the γ-, the ε- and the c-subunits during ATP synthesis and ATP hydrolysis. Specific attachment of one fluorophore to one of the rotating subunits and another fluorophore to a static subunit of F_oF_1-ATP synthase was applied, the enzyme was reconstituted into liposomes [34] and ATP synthesis was monitored in the presence of a high *pmf* [35]. Confocal detection of freely diffusing proteoliposomes provided smFRET time traces of catalytically active enzymes. Accordingly, rotation of the γ- and the ε-subunit in the catalytic F_1 domain occurred in three steps and in opposite direction for ATP synthesis compared to ATP hydrolysis, and proton-driven c-ring rotation was a ten-step movement. Moreover, catalytic turnover for each of the three binding sites was slightly different causing a "*kinetic limping*" [36]. Mean observation times of 20 to 100 ms in solution limited the detection of full rotations in single FRET-labeled enzymes to less than 4 rounds and required an analysis of dwell time histograms comprising all suitable accumulated rotary steps from different enzymes. Neither *static* nor *dynamic disorder* of turnover could be assessed. Averaged single-enzyme ATP synthesis rates were ~20 $ATP \cdot s^{-1}$, or ~70 $ATP \cdot s^{-1}$ for ATP hydrolysis, respectively, in agreement with ensemble measurements from biochemical assays of the same proteoliposomes.

Here, to analyze individual and variable catalytic turnover by single reconstituted F_oF_1-ATP synthases and to address the role of building up a *pmf* during ATP hydrolysis, observation times of proteoliposomes were extended using an Anti-Brownian electrokinetic trap (ABEL trap) in a microfluidic chip as developed by A. E. Cohen and W. E. Moerner [37]. Using smFRET as the readout, prolonged observation times allowed to record up to 100 full rotations of a single active enzyme in solution. The turnover changes of F_oF_1-ATP synthases followed the expected

concentration-dependence in the range from 5 µM to 1 mM ATP, but individual kinetic rates were broadly distributed for any ATP concentration and varied by a factor > 10, and the buildup of a *pmf* due to proton pumping limited ATP hydrolysis. The highest individual turnover of > 500 $ATP \cdot s^{-1}$ in the absence of a *pmf* exceeded the established average numbers from biochemical assays of F_oF_1-ATP synthases indicating that the promise of unraveling additional mechanistic insights by single-molecule enzymology still holds.

2. EXPERIMENTAL METHODS

Reconstituted FRET-labeled F_oF_1-ATP synthase. For smFRET recordings in the ABEL trap we prepared a specifically labeled enzyme. Briefly, we reassembled the purified F_1 part of F_oF_1-ATP synthase from *E. coli* with a cysteine mutation in the rotating ε-subunit at residue 56 (εH56C) [35b] with the reconstituted F_o part with a cysteine introduced at the C-terminus of the non-rotating *a*-subunit (*a*CT) [38]. Cy3B-maleimide was attached to εH56C with a labeling efficiency of 74 % as the FRET donor and Alexa Fluor 647-maleimide was attached to *a*CT with a labeling efficiency of 32 % as the FRET acceptor. The FRET-labeled reconstituted F_oF_1-ATP synthase was fully functional with a mean ATP synthesis rate of 16±2 $ATP \cdot s^{-1}$, i.e. in good agreement with similarly prepared FRET-labeled F_oF_1-ATP synthases [35b, 39]. A brief description of the purification procedures, labeling, reconstitution and catalytic activities of the FRET-labeled F_oF_1-ATP synthase is given in the Supporting Information online (Figures S1 to S6).

According to recent cryoEM structures of εCTD-inhibited *E. coli* F_oF_1-ATP synthase [40], the 120°-stepped rotation of the ε-subunit with respect to the static *a*-subunit will result in three distances between the C_α atoms of εH56C and *a*CT (Figure 1 A, B). Two short distances are 3.9 nm ("H_2", Figure 1 C) or 4.2 nm ("H_1", Figure 1 C), respectively, and a long distance is 7.2 nm ("L", Figure 1 C). In order to estimate FRET efficiencies corresponding to "L", "H_1" and "H_2", we used a Förster radius R_0=7.2 nm for the FRET pair Cy3B and Alexa Fluor 647, fluorescence quantum yields $\phi_{(Cy3B)}$=0.67 and $\phi_{(Alexa\ Fluor\ 647)}$=0.33 (data from "FPbase FRET calculator" at https://www.fpbase.org/fret) and considered an additional linker length of 0.5 nm for the fluorophores. Accordingly, two significantly different FRET efficiencies (E_{FRET}) are expected to be distinguishable in time traces of single enzymes during ATP-driven ε-subunit rotation, i.e. with

E_{FRET}=0.40 for "L" (or "medium FRET") and with E_{FRET}=0.93 for "H_1" or E_{FRET}=0.95 for "H_2" (both are "high FRET" and not distinguishable), respectively.

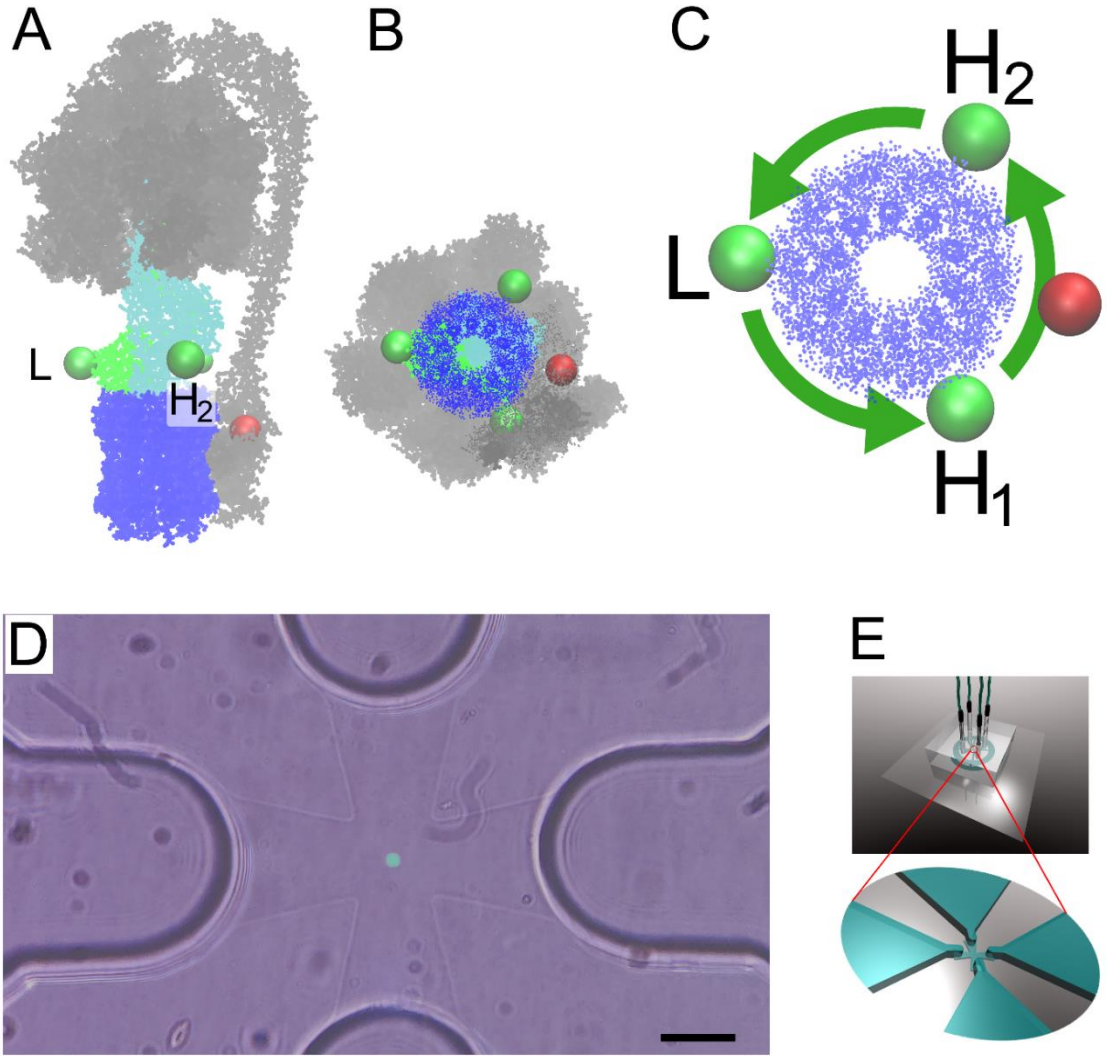

Figure 1. A-C, structure of *E. coli* F_oF_1-ATP synthase with cysteine mutations for labeling with FRET donor Cy3B on the rotating ε-subunit (green spheres) and FRET acceptor Alexa Fluor 647 on the static C-terminus of the *a*-subunit (red dot). **A**, side view with highlighted rotor subunits ε (green), γ (cyan) and c_{10}-ring (blue) and all static subunits in grey, based on PDB structure "6OQR" for the "L" orientation of ε and γ [40]. **B**, view from the bottom. **C**, assignment of FRET states "L", "H_1" and "H_2". During ATP hydrolysis, ε-subunit rotation in counter-clockwise direction will cause a FRET state sequence →"L"→"H1"→"H2"→"L"→. **D**, color image of the trapping region in the PDMS/glass chip of the ABEL trap with active 32-point laser pattern (green area, excitation 532 nm). Transitions from the cross-like 1 µm flat region to the 80 µm deep channels for the electrodes are visible. Black scale bar is 20 µM. **E**, scheme of the PDMS/glass chip with electrodes and magnified view of the trapping region (adopted from [41]).

ABEL trap for smFRET. The confocal ABEL trap for smFRET measurements comprised a 532 nm cw laser and two electro-optical beam deflectors to generate a 32-point knight tour pattern [37e]. The moving laser focus covered a 2.34x2.34 μm^2 area in the focal plane (see color image Figure 1D). The completed knight tour was repeated at 5 or 7 kHz rate and controlled by a field-programmable gate array (FPGA) card. The published FPGA-based ABEL trap software [37d] was slightly modified for utilizing up to four detectors in our setup [42]. Here we used the combined photon counts from two single photon counting avalanche photodiodes (APD), i.e. from FRET donor and FRET acceptor channel. The FPGA software directed the laser focus stepwise and recorded photons for each focus position. Once a fluorescent enzyme entered the trapping area, the software estimated the probable position of the proteoliposome and generated feed-back voltages to the four Pt electrodes to push the proteoliposome to the center of the focus pattern. The beam waist (from intensity maximum to the $1/e^2$ value) of the laser focus was 0.6 µm. The distance between adjacent focus positions was 0.47 µm ensuring an overlap between subsequent knight tour positions. An almost homogeneous illumination of the entire trapping area was achieved after time averaging the knight tour pattern for 1 ms. Using a 300 µm pinhole in the detection pathway in combination with the 60x oil immersion objective with a numerical aperture n.a. 1.42 allowed to detect all emitted photons from any position of the laser-excited area. Details of the setup are given in the Supporting Information.

Microfluidic PDMS sample chamber. The microfluidic chip to confine proteoliposome diffusion in two dimensions was made from structured PDMS bonded to cover glass after plasma etching (Figure 1E). Details of the preparation of PDMS/glass chips are given in the Supporting Information (Figure S7). The height in the trapping area was 1 µm, limiting the smFRET detection volume in the ABEL trap region of the chip to ~9 fL. The total volume of the chip including the 80 µm deep channels for the electrodes was ~10 µl. The design of the PDMS chip was adopted from previous publications [37c, 43]. To confirm the size of the detection volume, diffusion times of a diluted rhodamine 6 G solution (R6G) in H_2O were measured by fluorescence correlation spectroscopy (FCS). With a fixed laser focus position, the diffusion time of R6G was τ_D=0.35 ms. Applying the 32-point laser pattern in the absence of feed-back to the electrodes, the mean diffusion time increased 5-fold to τ_D~1.7 ms in agreement with the corresponding increase of the laser-excited area (Supporting Information Figure S8). Manual z-drift correction by lowering the microscope

objective to refocus the laser was necessary because of a continuing z-drift in the range of 1 µm in 5 to 10 minutes.

Analysis of smFRET traces. Proteoliposomes were diluted to a concentration of 20 to 50 pM F_oF_1-ATP synthases in the ABEL trap. FRET donor photons were detected in the spectral range between 544 nm and 620 nm and FRET acceptor photons with wavelengths $\lambda > 647$ nm. Using time-correlated single-photon counting (TCSPC) electronics with a time resolution of 164 ps, time traces were recorded for 25 min by multiplexing the APD signals for TCSPC in parallel to the FPGA input for ABEL trapping. The software "Burst Analyzer" [44] was used to visualize the fluorescence intensity time traces of FRET donor Cy3B, FRET acceptor Alexa Fluor 647 and the sum intensity on both detection channels. When a proteoliposome entered the trapping area, immediate trapping was characterized by a stepwise rise of the combined fluorescence count rate from 40 to 50 kHz above background within a single time bin of 1 ms. Photon bursts with lower or with higher total count rates were omitted from subsequent smFRET analyses. Loss from the trap or FRET donor photobleaching was accompanied by a stepwise drop of the total count rate to the background level. Photon bursts were manually marked, and background was subtracted for each photon burst individually because the background decreased on both channels in a time-dependent manner. Background decrease was caused by bleaching of impurities from within the PDMS and from the cover glass, for example, adsorbed fluorophores or adsorbed proteoliposomes within the trapping area. For each photon burst, the start time within the recording, its duration and the number of FRET state fluctuations were noted. A full 360° rotation of the ε-subunit with respect to the a-subunit of F_oF_1-ATP synthase comprised one "medium FRET" state plus one "high FRET" state, which corresponded to the supposed hydrolysis of 3 ATP molecules by the enzyme.

Photophysics of FRET donor and FRET acceptor fluorophores bound to F_oF_1-ATP synthase. In preliminary smFRET measurements of F_oF_1-ATP synthase in the ABEL trap we noticed that changing the excitation from 491 nm to longer wavelengths resulted in reduced background count rates using the PDMS/glass ABEL trap chips [42, 45]. To choose the optimal FRET donor for 532 nm excitation we compared the photophysical behavior of previously used tetramethylrhodamine (TMR) with Cy3B or Atto R6G bound to F_oF_1-ATP synthase. Reconstituted TMR-labeled enzymes exhibited a mean brightness of 14 kHz with a full width at half maximum (FWHM) of the brightness distribution of 4 kHz (Supporting Information Figure S9). The trapping times of the

enzymes varied. The maximum of the photon burst duration distribution was around 200 ms, with few bursts lasting up to 2 seconds. Fitting the distribution with an exponential decay function yielded an average duration of 350 ms. The reconstituted Cy3B-labeled F_oF_1-ATP synthase exhibited a much higher mean brightness of 34 kHz, with a FWHM of the brightness distribution of 5 kHz (Supporting Information Figure S9). The photon burst duration distribution differed and comprised longer trapping times. The average duration was prolonged to 750 ms. Background was comparable to the measurements of the TMR-labeled enzyme, i.e. decreased from 15 kHz at the beginning to 10 kHZ within 5 min. Alternatively we examined AttoR6G as a FRET donor. AttoR6G-labeled reconstituted enzymes exhibited a mean brightness of 41 kHz, i.e. higher than Cy3B or TMR. The intensity distribution was asymmetrically broadened with a FWHM of 8 kHz (Supporting Information Figure S9). The duration distribution was comparable to TMR-labeled F_oF_1-ATP synthases, with few bursts lasting up to 2.5 seconds, yielding an average duration of 370 ms for trapped proteoliposomes.

Therefore, we chose Cy3B on the ε-subunit as the FRET donor because of its relatively high single-molecule brightness, the narrow and symmetric brightness distribution confirming a lack of protein-induced fluorescence changes [46] and its significantly prolonged residence times in the ABEL trap. Selecting Alexa Fluor 647 as the FRET acceptor provided a large Förster radius R_0 and allowed to test the use of a triplet quencher in order to increase the brightness or to diminish blinking of both fluorophores [47].

3. RESULTS AND DISCUSSION

Reassembly of Cy3B-labeled F_1 domains to the Alexa Fluor 647-labeled F_o domain of the enzyme in a liposome yielded a fully functional F_oF_1-ATP synthase which synthesized ATP from ADP and phosphate with a catalytic rate of 16 $ATP \cdot s^{-1}$ (Supporting Information, Figure S6) in good agreement with our previous rebinding results of F_1 domains onto F_o domains in liposomes [35b, 38a].

Two distinct FRET states in the presence of AMPPNP. AMPPNP is the non-hydrolyzable ATP derivative which binds with similar affinity to *E. coli* F_oF_1-ATP synthase but stalls the γ-, *c*- and ε-

subunit rotation, i.e. results in a rotor orientation in one of three angular positions with respect to the *a*-subunit of the peripheral stalk. For single-molecule measurements in the ABELtrap, the proteoliposome suspension was diluted to an enzyme concentration of approximately 20 pM in buffer (10 mM tricine, 10 mM succinate, 0.3 mM KCl, pH 8.0) containing 1.25 mM Mg^{2+} and 1 mM AMPPNP. Figure 2 shows examples of individual ABEL trapped F_oF_1-ATP synthases. The actual mean background photon counts on both detector channels had been subtracted and FRET was calculated using the proximity factor $P=I_{acceptor}/(I_{donor} + I_{acceptor})$ instead of a fully corrected FRET efficiency. Most photon bursts (i.e. 84% of 1593) were not exhibiting a FRET acceptor signal and were called "donor only"-labeled enzymes (see photon bursts with numbers I, V, VI, VII in Figure 2 A). Due to spectral crosstalk of Cy3B emission into the FRET acceptor channel, the mean apparent proximity factors of the "donor only" photon bursts were P=0.15±0.05. However, enzymes with distinct P values of 0.4 (medium FRET, photon burst II) or P>0.8 (high FRET, photon bursts III, IV) were also found. In photon burst IV, the FRET acceptor Alexa Fluor 647 (red trace) photobleached after 90 ms but the proteoliposome remained trapped due to the FRET donor signal (green trace). Figure 2 B shows another enzyme with mean P~0.4, hold in solution by the ABELtrap for 4.3 seconds. Figure 2 C shows an enzyme with mean P~0.9 hold for 1.4 seconds, with FRET acceptor photobleaching near the end of this photon burst.

The histogram of P values from all FRET-labeled F_oF_1-ATP synthases in Figure 2 D indicated two subpopulations with comparable occurrence, and the two FRET states were well separated. The P~0.4 state was associated with higher total photon counts for the sum of FRET donor and acceptor signals (~37 kHz in Figure 2 E) in comparison to the P~0.85 state with ~20 kHz. The "donor only" state with apparent P~0.15 exhibited about 45 kHz as added intensities from both detection channels (Supporting Information, Figure S11). Sum photon signals were depicted as black traces in Figures 2 A-C. The FRET state duration depended on the proximity factor, i.e. FRET states with medium P values lasted longer (Figure 2 F), with similar lengths up to 5 seconds as "donor only" photon bursts (Supporting Information, Figure S11). FRET states with high P values were found remaining up to 2 seconds. As FRET acceptor photobleaching was observed for both medium and high P, the difference in FRET state duration could be caused by faster Alexa Fluor 647 bleaching in the high FRET state or by predominant loss from the trap of FRET-labeled enzymes with lower total photon count rates and, accordingly, an unfavorable signal-to-background ratio.

To enhance the photostability of the cyanine dye Alexa Fluor 647 we tested an addition of the antioxidant 6-hydroxy-2,5,7,8-tetramethylchroman-2-carboxylic acid ("*trolox*", [48]) to the buffer in the presence of 1 mM AMPPNP. In the presence of 2 mM "*trolox*", AMPPNP-stalled F_oF_1-ATP synthases showed the same two proximity factor states P~0.4 and P~0.85, and about 80% of the enzymes were found as "donor only"-marked (Supporting Information, Figure S11). The apparent proximity factor of the "donor only" photon bursts was P=0.15±0.05 (Supporting Information, Figure S11). Slightly different brightnesses of individual FRET donor Cy3B were recognized in the presence of "*trolox*". Cy3B-labeled F_oF_1 ATP synthases emitted between 45 kHz and 35 kHz resulting in a broadened distribution of summed-intensity-*versus* P values (Supporting Information, Figure S11). However, the apparent proximity factor remained the same, i.e. FRET donor brightness did not affect the P values. Importantly, the distribution of FRET state durations did not display a significant prolongation but was similarly to photon bursts in the absence of the antioxidant "*trolox*". Adding 2 mM "*trolox*" yielded no obvious photophysical improvement for the smFRET recording in the ABEL trap.

Two fluctuating FRET states in the presence of 1 mM ATP. To monitor catalytic turnover of F_oF_1-ATP synthase, 1 mM ATP, i.e. at a saturating concentration and in the presence of 1.25 mM Mg^{2+}, was added to the proteoliposomes. Although many enzymes showed a constant FRET efficiency with proximity factors of either P~0.4 or P~0.85, we also observed many photon bursts with fast oscillating FRET levels (Figure 3) caused by anticorrelated changes of FRET donor and acceptor signals. As these fluctuations were not observed in the absence of ATP, we attributed these FRET fluctuations to ε-subunit rotation driven by ATP hydrolysis. FRET fluctuations were analyzed as pairs of one medium FRET level (P<0.5) plus one high FRET level (P>0.8) in the time trace. Each FRET pair was interpreted to represent a full 360° rotation of the ε-subunit because the two different high FRET level "H_1" and "H_2" were expected to be too similar and indistinguishable for short FRET level durations. Accordingly, one pair of FRET level was correlated with 3 hydrolyzed ATP molecules.

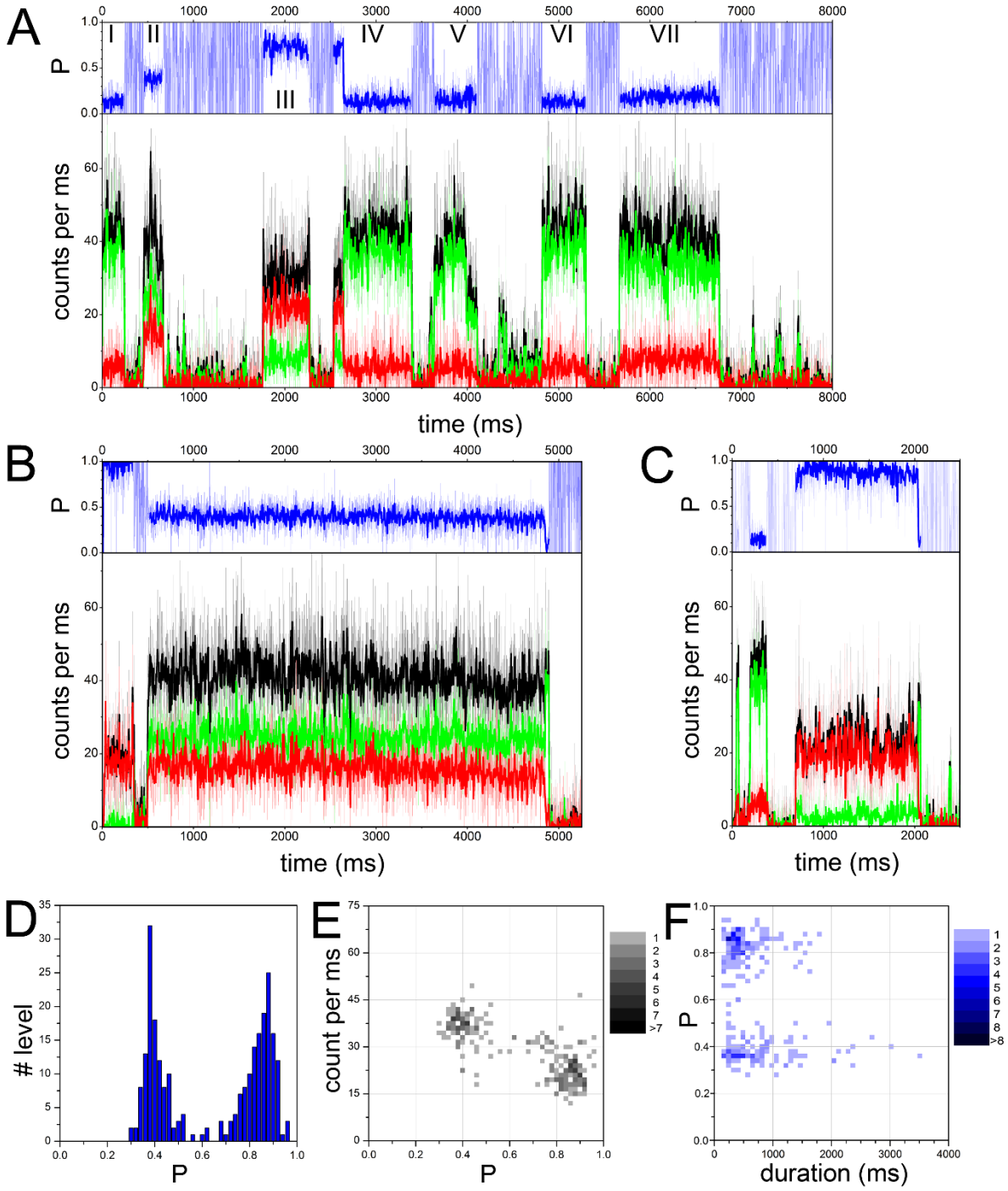

Figure 2. **A-C**, Photon bursts of reconstituted F_oF_1-ATP synthases labeled with Cy3B (green intensity trace) and Alexa Fluor 647 (red intensity trace) and hold in the ABEL trap in the presence of 1 mM AMPPNP. Black traces are summed intensities. Blue traces above are the calculated proximity factor values. Time bin is 1 ms for the thin line traces and 5 ms for the bold traces. **D**, proximity factor P distribution of the FRET-labeled enzymes. **E**, 2D histogram of mean total brightness (sum intensities from both FRET donor and acceptor signals) *versus* P. **F**, 2D histogram of P *versus* photon burst duration. ----------

Manual assignment of beginning and end of FRET fluctuations within a photon burst and counting the number of FRET pairs within the photon burst allowed to assign a mean catalytic rate, or ATP hydrolysis rate, respectively, for each individual FRET-labeled F_oF_1-ATP synthase hold by the ABEL trap. For example, the enzyme shown in Figure 3A exhibited 74 FRET fluctuations (or pairs of FRET level) within an 1118 ms period before the FRET acceptor Alexa Fluor 647 photobleached and then the enzyme remained as a "donor only"-labeled F_oF_1-ATP synthase trapped for another 327 ms. The number of full rotations per period corresponded to an average of 15.1 ms per 3 hydrolyzed ATP molecules and a mean ATP hydrolysis rate of 199 $ATP \cdot s^{-1}$. This enzyme was recorded 6 min after starting the ABEL trap measurement.

In Figure 3B another enzyme is depicted that was recorded 11.4 min after starting the ABEL trap measurement. Here, the FRET fluctuations occurred significantly slower and with a clear stepwise change between the medium and high FRET level. Within 1250 ms duration, 17 FRET level pairs were assigned, corresponding to 73.5 ms per full rotation and a mean ATP hydrolysis rate of 41 $ATP \cdot s^{-1}$. After FRET acceptor photobleaching the "donor only"-labeled enzyme remained trapped for another 386 ms.

The rotational speed varied from enzyme to enzyme. However, some trapped enzymes exhibited also an apparent change of the catalytic rate within the FRET fluctuation period. In Figure 3C the mean catalytic rate was ~60 $ATP \cdot s^{-1}$, but the first FRET fluctuation period of this F_oF_1-ATP synthase was slower with a mean of 36 $ATP \cdot s^{-1}$ during 1264 ms and followed by a faster period with 108 $ATP \cdot s^{-1}$ for 417 ms. This enzyme was recorded 9 min after starting the ABEL trap measurement. A second example of dynamic changes of the catalytic rate of F_oF_1-ATP synthase is shown is Figure 3D. In the first part, i.e. for 342 ms, the rate was very fast with 347 $ATP \cdot s^{-1}$, then turnover slowed down to 64 $ATP \cdot s^{-1}$ for 235 ms, and accelerated in the second half of the photon burst to 190 $ATP \cdot s^{-1}$ before the FRET acceptor photobleached. This enzyme was recorded 5.3 min after starting the ABEL trap measurement.

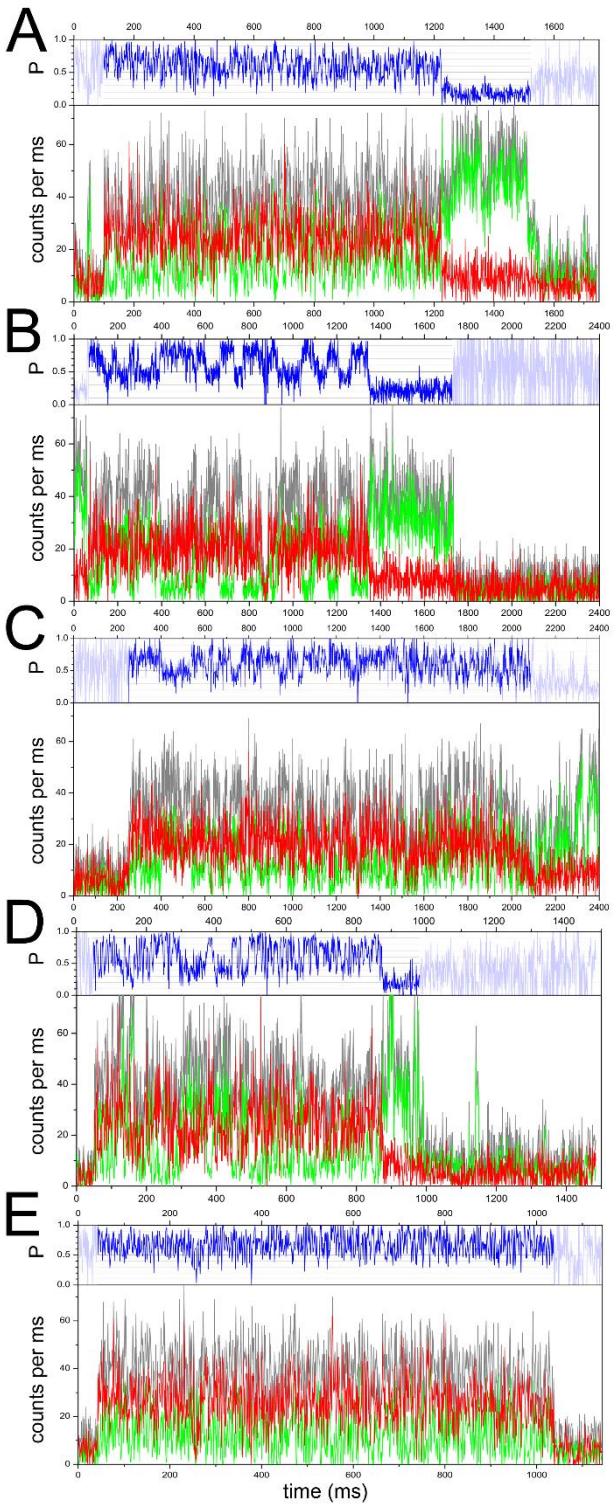

Figure 3. **A-E**, five photon bursts of reconstituted F_oF_1-ATP synthases labeled with Cy3B and Alexa Fluor 647 and hold in the ABEL trap in the presence of 1 mM ATP. Photon counts from FRET donor in green, FRET acceptor in red, sum intensity in grey, and proximity factor P in blue. Time binning is 1 ms. P values before and after the photon bursts of the trapped enzymes were shaded for clarity. ----------

In addition, enzymes with much faster FRET fluctuations were observed. For the F_oF_1-ATP synthase shown in Figure 3E a mean ATP hydrolysis rate 356 ATP·s^{-1} was calculated from 118 rotations in 994 ms. This enzyme was recorded 4 min after starting the ABEL trap measurement.

Distribution of catalytic rates from individual enzymes in the presence of 1 mM ATP. The wide range of ATP-driven rotation rates in single F_oF_1-ATP synthases was analyzed with respect to the time of ATP addition to the proteoliposomes or the start of the smFRET recording with ABEL trapping, respectively. A series of five independent measurements were combined in Figure 4 A and indicated no trends in the distribution of catalytic rates, with each recording spanning the time course of 25 min. From start to end the individual mean ATP hydrolysis rate scattered between 20 ATP·s^{-1} to 400 ATP·s^{-1} in the presence of 1 mM ATP (Figure 4 A, left diagram). The rate distribution had a broad maximum in the range of 100 to 200 ATP·s^{-1} (Figure 4 A, middle diagram). No correlation could be found between the number of rotations per photon burst and the associated ATP hydrolysis rate (Figure 4 A, right diagram), excluding a bias from enzymes with a longer duration in the ABEL trap and, therefore, more rotations. The ATP hydrolysis rate distribution was essentially determined by photon bursts with less than 20 rotations. Only 2 from a total number of 289 single F_oF_1-ATP synthases were recorded with more than 100 full rotations. The different rotational speed or different catalytic rate from enzyme to enzyme is called *static disorder* whereas the variation of catalytic speed including a stop-and-go behavior within a single enzyme is called *dynamic disorder* [18].

ATP-concentration dependent catalytic rates from 5 µM to 1 mM ATP. We repeated the measurements of individual ATP hydrolysis rates using different lower ATP concentrations, i.e. in the presence of either 100 µM ATP, 40 µM ATP, 20 µM ATP and 5 µM ATP. Examples of photons bursts at all ATP concentrations are given in the Supporting Information (Figures S12 and S13). Fast and slow catalytic turnover was observed at any ATP concentration, as calculated from the pairs of medium and high FRET levels. The transition between the P~0.4 and P~0.85 levels occurred fast in the range of one to a few ms. However, at 5 µM ATP these transitions became longer in some photon bursts, and occurred either in a continuous, "ramp-like" behavior, or stepwise but the high FRET level was split into two distinct high FRET level at P>0.85 and at 0.6<P<0.8 (Supporting Information, Figure S13).

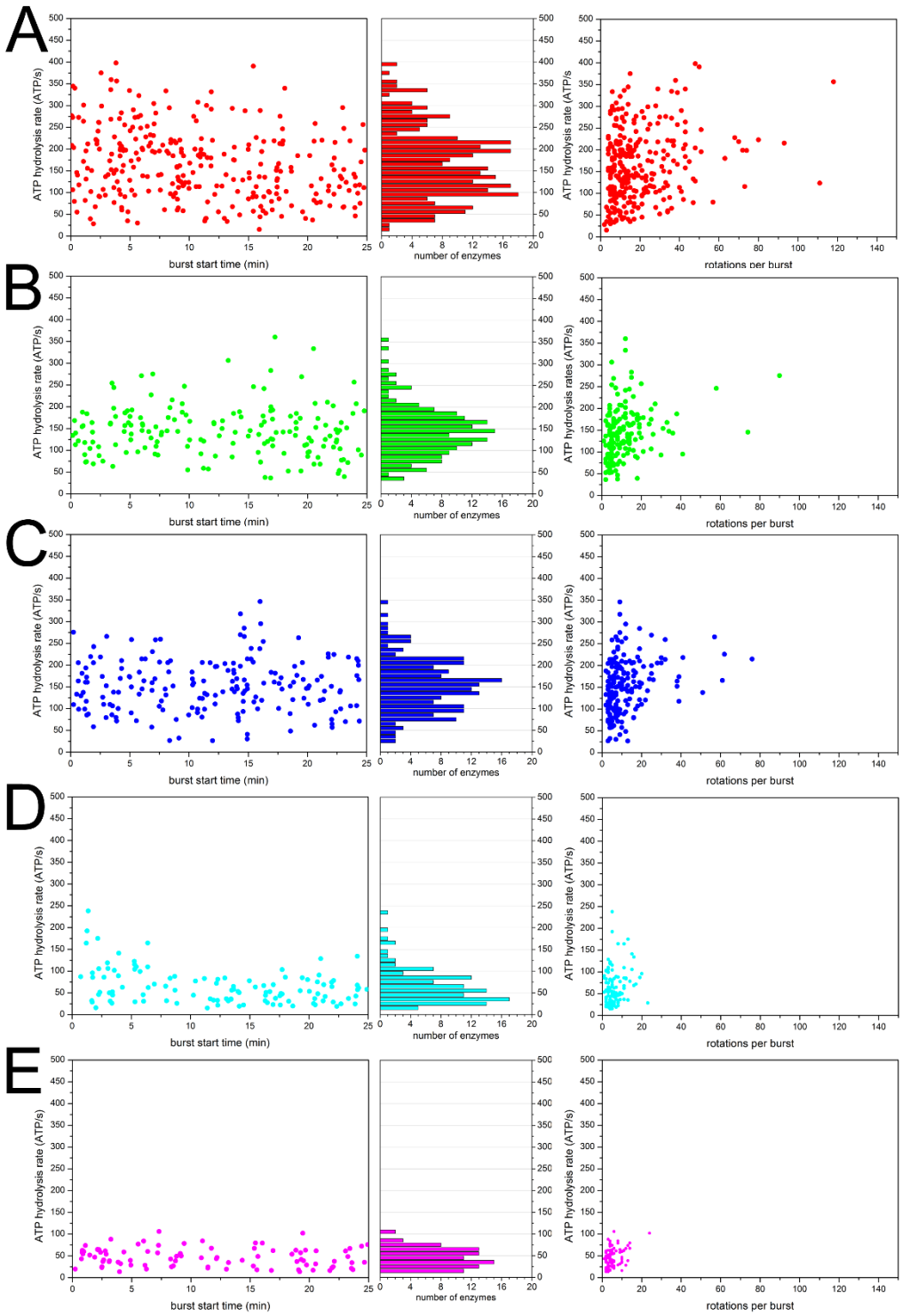

Figure 4. Distributions of individual ATP hydrolysis rates for FRET-labeled F_oF_1-ATP synthases for five ATP concentrations. **A**, 1 mM ATP, **B**, 100 µM ATP, **C**, 40 µM ATP, **D**, 20 µM ATP, **E**, 5 µM ATP. **Left diagrams**, time-dependence of individual catalytic rates, **middle diagrams**, histograms of rates, **right diagrams**, relation of the counted number of rotations during the FRET fluctuation period and the associated ATP hydrolysis rates. ----------

The single-enzyme rate distributions were summarized in Figure 4. For each ATP concentration the catalytic rates varied substantially by factor 10 at 100 µM ATP (i.e. between 36 $ATP \cdot s^{-1}$ to 360 $ATP \cdot s^{-1}$ for 175 enzymes), factor 13 at 40 µm ATP (i.e. between 27 $ATP \cdot s^{-1}$ to 346 $ATP \cdot s^{-1}$ for 184 enzymes), factor 16 at 20 µM ATP (i.e. between 15 $ATP \cdot s^{-1}$ to 238 $ATP \cdot s^{-1}$ for 112 enzymes), and factor 8 at 5 µM ATP (i.e. between 14 $ATP \cdot s^{-1}$ to 106 $ATP \cdot s^{-1}$ for 89 enzymes). No time-dependent decrease of catalytic rates was observed even for the low ATP concentrations, i.e. the initial substrate concentrations were not altered significantly by the enzymatic turnover within the 25 min recording time. However, at 20 µM and at 5 µM ATP, the average individual ATP hydrolysis rates of F_oF_1-ATP synthases were smaller than those at the higher ATP concentrations, as expected from basic enzyme kinetics and biochemical assays.

Consistent with the ATP-dependent decrease of mean catalytic turnover, the maximum number of rotations per FRET fluctuation period decreased with lower substrate concentration from about 90 rotations at 100 µM ATP to around 15 at 5 µM ATP (right diagrams in Figure 4). The distributions of FRET fluctuation durations were similar for all ATP concentrations with upper limits between 1 to 1.5 seconds (Supporting Information, Figure S14).

Dissipating the *pmf* with ionophores. A possible cause for the broad distributions of catalytic rates could be a variable pH gradient and electric membrane potential for each proteoliposome. Due to the stochastic ATP-driven proton pumping by F_oF_1-ATP synthase, the actual ΔpH and membrane potential might counteract ATP hydrolysis differently in individual proteoliposomes. Therefore, the addition of ionophores and uncouplers was investigated (Figure 5). First, in the presence of 100 µM ATP, the effect of the protonophore carbonyl cyanide m-chlorophenyl hydrazone (CCCP, 50 µM) was measured. FRET-labeled F_oF_1-ATP synthases were observed with fast transitions between the medium and high FRET level. The enzyme in Figure 5 A hydrolyzed ATP with a rate of 418 $ATP \cdot s^{-1}$. The individual ATP hydrolysis rates for different enzymes varied between 112 $ATP \cdot s^{-1}$ to 537 $ATP \cdot s^{-1}$ by factor 5 (Figure 5 B). The average ATP hydrolysis rate from all enzymes was 354 $ATP \cdot s^{-1}$, i.e. the mean turnover was 2.5-fold faster than for 100 µM ATP (144 $ATP \cdot s^{-1}$, Figure 4 B) without the protonophore CCCP. Apparently a slightly slower mean turnover towards the end of the 25 min recording time could be estimated.

As an alternative to CCCP, the combination of valinomycin acting as a K^+ carrier across the lipid bilayer and nigericin acting as an antiporter for H^+ and K^+ was measured at 1 µM concentration of each and with 100 µM ATP present. Fast transitions between the medium and high FRET level were observed in FRET-labeled F_oF_1-ATP synthases. The enzyme shown in Figure 5 C exhibited 117 full rotations in 1027 ms, i.e. a catalytic rate of 342 ATP·s^{-1}. Individual ATP hydrolysis rates varied between 111 ATP·s^{-1} to 496 ATP·s^{-1} by factor 5 (Figure 5 D). The average ATP hydrolysis rate from all enzymes was 295 ATP·s^{-1}, i.e. the mean turnover was twofold faster than in the presence of 100 µM ATP solely. A twofold increase of average ATP hydrolysis rates in biochemical assays in the presence of valinomycin and nigericin was observed previously using *E. coli* F_oF_1-ATP synthases reconstituted in liposomes [13].

The distributions of all individual F_oF_1-ATP synthase turnover numbers are combined in the box-and-whisker plots in Figure 5 E. As defined, the lower limit of each box was constructed from the 25% threshold (1st quartile) of the ATP hydrolysis data and the upper limit from the 75% threshold (3rd quartile). The median of all the rate distributions, i.e. the horizontal line within the interquartile range, was almost identical to the mean value of each set (dot in the box). The data sets recorded in the presence of 100 µM ATP showed that the interquartile ranges of turnover numbers for the measurements without (green box) and with uncouplers CCCP (dark yellow box) or valinomycin plus nigericin (yellow box) did not overlap, i.e. single-enzyme catalytic rates were significantly higher in the presence of uncouplers. These distinct distributions confirmed that the buildup of a ΔpH and an electric membrane potential, i.e. a *pmf* by ATP-driven proton pumping into the proteoliposomes, slowed down ATP turnover of F_oF_1-ATP synthase. However, the ranges defined by the whiskers (i.e. lines extending the box) of the distributions in the presence of uncouplers still overlap with the interquartile range for 100 µM ATP (green box) revealing that dissolving the *pmf* by uncouplers is not sufficient to minimize the wide variability of the rate distributions. Only a few outliers (single data points below and above the whiskers in Figure 5 E) were identified in each data set of ATP hydrolysis rates but few enzymes with very fast ATP turnover >300 ATP·s^{-1} were found at 1 mM ATP, at 100 µM ATP and at 40 µM ATP.

For the lower ATP concentrations 20 µM (cyan box) and 5 µM (purple box) their interquartile ranges did not overlap with the other boxes (red, green, blue), indicating that catalytic turnover on

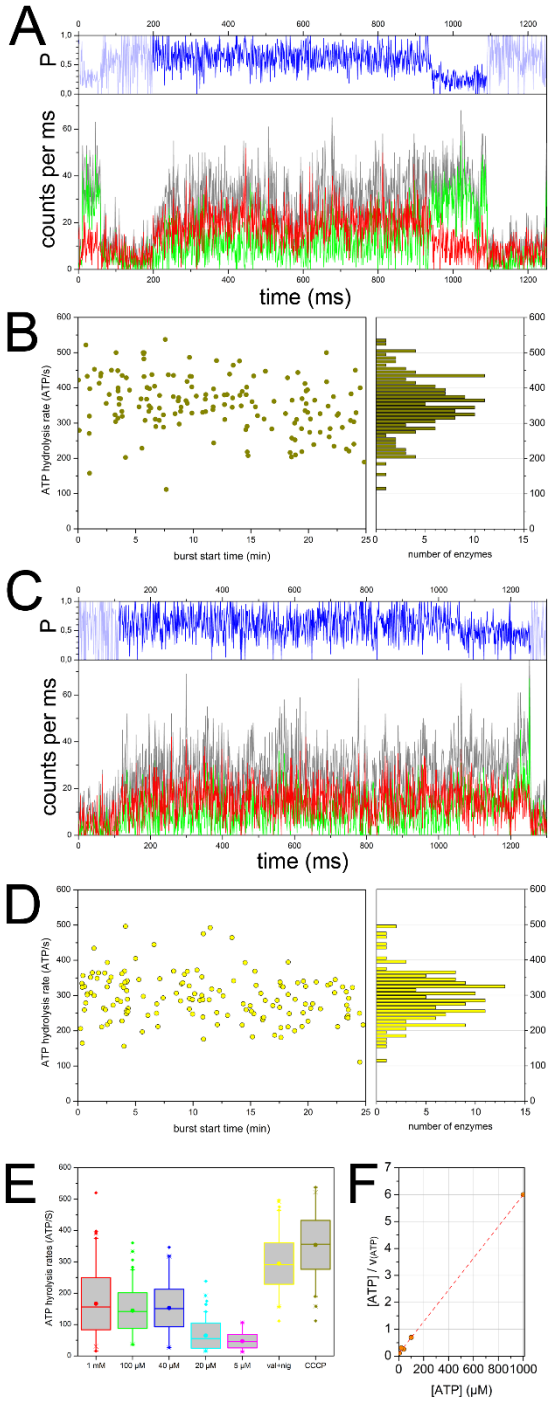

Figure 5. Photon bursts of reconstituted F_oF_1-ATP synthases in the presence of 100 µM ATP and either 50 µM protonophore CCCP (**A**) or uncouplers 1 µM valinomycin and 1 µM nigericin (**C**). **B**, time-dependent distribution of individual ATP hydrolysis rates with CCCP. **D**, time-dependent distribution of individual ATP hydrolysis rates with valinomycin plus nigericin. **E**, box-and-whisker plot of all individual ATP hydrolysis rates at different ATP concentration and with CCCP or valinomycin plus nigericin. **F**, Hanes-Woolf plot for ATP-dependent hydrolysis rates using the median values from figure **E**.----------

average was significantly slower. We tested the possibility to obtain kinetic parameters from the median values of the ATP-dependent distributions according to the Michaelis-Menten theory. Using the Hanes-Woolf linearization [49] in Figure 5 F, the maximum ATP hydrolysis rate $V_{(max)}$= 169 ATP·s^{-1} was calculated from the slope of the fit (red line). The Michaelis-Menten constant K_m= 17 µM was calculated from the intercept and from $V_{(max)}$. Alternatively, using the Lineweaver-Burk linearization [50] $V_{(max)}$=147 ATP·s^{-1} and K_m= 12 µM was calculated (Supporting Information, Figure S15). These $V_{(max)}$ values of reconstituted F_oF_1-ATP synthases were smaller than $V_{(max)}$=651 ATP·s^{-1} or $V_{(max)}$=516 ATP·s^{-1} reported for single enzymes solubilized in detergent, attached to a glass surface, and measured at room temperature using dark-field microscopy [51]. The smFRET-based $V_{(max)}$ and K_m were in agreement with biochemical assays of *E. coli* F_oF_1-ATP synthase using native membrane vesicles ($V_{(max)}$~200 ATP·s^{-1} [7], $V_{(max)}$=336 ATP·s^{-1} at 30°C [52]), purified enzymes in detergent ($V_{(max)}$=285 ATP·s^{-1} and K_m=78 µM at 24°C [5], $V_{(max)}$=217 ATP·s^{-1} and K_m=140 µM at 30°C [53], $V_{(max)}$=700 ATP·s^{-1} with 10 mM ATP and 5 mM Mg^{2+} at 37°C [54]), single enzymes reconstituted into lipid nanodiscs ($V_{(max)}$=140 ATP·s^{-1} at 25°C [12]) or purified enzymes reconstituted into liposomes (v=65 ATP·s^{-1} at 100 µM ATP, increasing to v=210 ATP·s^{-1} in the presence of uncouplers valinomycin and nigericin [11, 13]). $V_{(max)}$ obtained from Figure 5 F was about twice as fast as the mean turnover of ~70 ATP·s^{-1} at 1 mM ATP reported previously in single-molecule FRET experiments with reconstituted F_oF_1-ATP synthase in solution [35b, 39, 55]. However, in the previous smFRET experiments dwell times of FRET levels from all active enzymes had to be combined before fitting because short observation times of freely diffusing proteoliposomes resulted in a few turnovers per enzyme only. For the actual ABEL trap data analysis, the turnover of each enzyme could be calculated separately based on many full rotations, before sorting the individual rates into the histograms.

The maximum speed of subunit rotation in reconstituted F_oF_1-ATP synthase and causes for static and dynamic disorder. The maximum catalytic rates for surface-attached single F_1 fragments (1350 ATP·s^{-1} [56] or 2160 ATP·s^{-1} [30] at room temperature) were not reached with reconstituted *E. coli* F_oF_1-ATP synthases in the ABEL trap. Undisturbed from any surface-related interference the maximum ATP hydrolysis rate of a single enzyme in the presence of 1 mM ATP was 400 ATP·s^{-1}. However, under the same substrate conditions enzymes were recorded exhibiting a much slower turnover of 20 ATP·s^{-1}. The wide variation of individual catalytic rates did not change during the recording time and the heterogeneities occurred for all ATP turnover conditions.

This heterogeneity of catalytic activity from one enzyme to the next had been called *static disorder* [18], observable only by single-molecule enzymology. To elucidate the causes of catalytic heterogeneities between individual enzymes and within a turnover time trace (*dynamic disorder*), we reconsider the spatial and the temporal uniformness of the local environment of the F_oF_1-ATP synthase.

First, the reconstitution approach with re-attaching the FRET donor Cy3B-labeled F_1 domain back onto the FRET acceptor Alexa Fluor 647-labeled F_o domain in liposomes allowed to circumvent analyzing any F_oF_1-ATP synthase with a wrong outside-in orientation, because the F_1 domain can only bind to the correctly inserted F_o domain. Because we analyzed ATP-driven FRET fluctuations only, all inactive enzymes were excluded and their fraction did not influence the kinetic results.

Second, holding single proteoliposomes in solution by the ABEL trap allowed to record smFRET time traces of *E. coli* F_oF_1-ATP synthase during ATP hydrolysis in an isotropic environment and for up to two seconds. The diameter of a proteoliposome in the range of 150 nm was small with respect to the 1.1 µm height of the trapping region of the PDMS/glass sample chamber. Therefore, diffusion of the substrate ATP to the enzyme and the products ADP and phosphate from the enzymes was not spatially restricted in the trap. During each 25 min recording time, a systematic change or an average slowdown of the turnover was not found. ATP consumption by the enzymes, diluted to ~50 pM, was negligible, so that the temporal uniformness of substrate and products for the catalytic turnover was ensured.

Third, one cause of *static disorder* for reconstituted F_oF_1-ATP synthase is the buildup of a *pmf* counteracting the ATP hydrolysis reaction. Adding protonophores or uncouplers revealed enzymes with a faster maximum ATP hydrolysis rate up to 537 $ATP \cdot s^{-1}$ supporting that a *pmf* is limiting catalysis. Adding saturating uncoupler concentrations did not result in narrow turnover distributions, so that future smFRET rotation experiments might require F_oF_1-ATP synthase reconstituted in a lipid nanodisc in order to prevent any residual *pmf* as the cause of *static disorder*.

Finally, the regulatory mechanism for ATP hydrolysis in F_oF_1-ATP synthase, i.e. conformational changes of the εCTD to mechanically inhibit the motion of the γ, ε and c-ring rotor, might contribute to the *static disorder* as well as the *dynamic disorder*. Beyond the extended εCTD

conformation[57] ("up") to block rotary catalysis and the compact active "down" conformation[58], intermediate and different extension states of the εCTD have been reported for the *E. coli* enzyme [59], and the transition times between them are unknown. Depending on the time scale of conformational changes of the ε mutants, slow changes could be related to the *static disorder* observed for different enzymes, or fast changes could explain the *dynamic disorder* within the time trace of individual catalytically active enzymes. To unravel the role of εCTD conformations for the catalytic heterogeneities of F_oF_1-ATP synthase in the future, catalysis of truncation mutants will be analyzed by smFRET in the ABEL trap, for example the ε91-stop mutant with a complete removal of the εCTD [5] and the εΔ5 mutant with the last 5 amino acids removed [9]. *Vice versa*, direct FRET monitoring of the εCTD conformation in single enzymes could be applied to obtain the time constants of εCTD movements.

Most recently, cryoEM structures provided evidence for an additional relative movement of the ε-subunit [60]. A subpopulation exhibited a rotary shift of about 60°, but the εCTD was found an active "down" conformation, which was interpreted as a conformation related to the ADP-inhibited state. As very rare events, we have found FRET-labeled enzymes with a intermediate proximity factor P~0.6 that was long-lasting and almost static, which might represent these postulated novel ADP-inhibited conformations. Unraveling these regulatory conformational dynamics is required to fully understand how the membrane enzyme works in both catalytic reaction directions, i.e. ATP synthesis and ATP hydrolysis. This information will be accessible by single-molecule spectroscopy, briefly by smFRET in isotropic solution to avoid surface-related artefacts, and the ABEL trap will be the essential tool to record long time trajectories of active F_oF_1-ATP synthase at work.

4. ACKNOWLEDGMENT

The authors thank A. E. Cohen and W. E. Moerner for liberally providing detailed design and laboratory protocols, the complete measurement software and multiple hardware advice to setup an ABEL trap. We thank all members of the single-molecule microscopy group who participated in biochemistry, and especially thank T. Rendler, N. Zarrabi, B. Su, M. Dienerowitz and A. Dathe who assembled different versions of the ABEL trap. The ABEL trap was realized by funds from

the "Deutsche Forschungsgemeinschaft" DFG (grants BO1891/10-2, BO1891/15-1, BO1891/16-1, BO1891/18-2 to M.B.) and was supported by an ACP Explore project (M.B. together with J. Limpert) within the ProExcellence initiative ACP2020 from the State of Thuringia.

5. ASSOCIATED CONTENT

Supporting Information. An associated PDF file with 15 supplemental figures is available free of charge online, comprising preparation of FRET-labeled F_oF_1-ATP synthase from *E. coli* including fluorophore labeling, reconstitution, catalytic activity measurements of ATP hydrolysis and synthesis, the confocal ABEL trap setup, PDMS/glass sample chamber preparation, photophysics of FRET fluorophores bound to the enzyme with and without the antioxidant "trolox", photon bursts of single FRET-labeled F_oF_1-ATP synthases in the presence of 100 μM ATP, 40 μM ATP, 20 μM ATP and 5 μM ATP, distributions of fluctuating FRET level durations, Lineweaver-Burk analysis of smFRET-based ATP hydrolysis rates.

6. REFERENCES

1. Ogura, Y., Catalase activity at high concentration of hydrogen peroxide. *Arch Biochem Biophys* **1955,** *57* (2), 288-300.
2. Pearson, M. A.; Park, I. S.; Schaller, R. A.; Michel, L. O.; Karplus, P. A.; Hausinger, R. P., Kinetic and structural characterization of urease active site variants. *Biochemistry* **2000,** *39* (29), 8575-84.
3. Lane, A. N.; Kirschner, K., Mechanism of the physiological reaction catalyzed by tryptophan synthase from Escherichia coli. *Biochemistry* **1991,** *30* (2), 479-84.
4. (a) Mitchell, P., Coupling of phosphorylation to electron and hydrogen transfer by a chemi-osmotic type of mechanism. *Nature* **1961,** *191*, 144-8; (b) von Ballmoos, C.; Wiedenmann, A.; Dimroth, P., Essentials for ATP synthesis by F1F0 ATP synthases. *Annu Rev Biochem* **2009,** *78*, 649-72.
5. Iino, R.; Hasegawa, R.; Tabata, K. V.; Noji, H., Mechanism of inhibition by C-terminal alpha-helices of the epsilon subunit of Escherichia coli FoF1-ATP synthase. *The Journal of biological chemistry* **2009,** *284* (26), 17457-64.
6. Fischer, S.; Graber, P., Comparison of ΔpH- and Δψ-driven ATP synthesis catalyzed by the H(+)-ATPases from Escherichia coli or chloroplasts reconstituted into liposomes. *FEBS letters* **1999,** *457* (3), 327-32.
7. Etzold, C.; Deckers-Hebestreit, G.; Altendorf, K., Turnover number of Escherichia coli F0F1 ATP synthase for ATP synthesis in membrane vesicles. *European journal of biochemistry / FEBS* **1997,** *243* (1-2), 336-43.
8. Tsunoda, S. P.; Aggeler, R.; Yoshida, M.; Capaldi, R. A., Rotation of the c subunit oligomer in fully functional F1Fo ATP synthase. *Proceedings of the National Academy of Sciences of the United States of America* **2001,** *98* (3), 898-902.

9. Shah, N. B.; Duncan, T. M., Aerobic growth of *Escherichia coli* is reduced and ATP synthesis is selectively inhibited when five C-terminal residues are deleted from the ε subunit of ATP synthase. *Journal of Biological Chemistry* **2015,** *290*, 21032-21041.
10. Meyrat, A.; von Ballmoos, C., ATP synthesis at physiological nucleotide concentrations. *Sci Rep* **2019,** *9* (1), 3070.
11. Fischer, S.; Graber, P.; Turina, P., The activity of the ATP synthase from Escherichia coli is regulated by the transmembrane proton motive force. *The Journal of biological chemistry* **2000,** *275* (39), 30157-62.
12. Ishmukhametov, R.; Hornung, T.; Spetzler, D.; Frasch, W. D., Direct observation of stepped proteolipid ring rotation in E. coli F(0)F(1)-ATP synthase. *The EMBO journal* **2010,** *29* (23), 3911-23.
13. Lapashina, A. S.; Prikhodko, A. S.; Shugaeva, T. E.; Feniouk, B. A., Residue 249 in subunit beta regulates ADP inhibition and its phosphate modulation in Escherichia coli ATP synthase. *Biochimica et biophysica acta. Bioenergetics* **2019,** *1860* (3), 181-188.
14. (a) Milgrom, Y. M.; Duncan, T. M., F-ATP-ase of Escherichia coli membranes: The ubiquitous MgADP-inhibited state and the inhibited state induced by the epsilon-subunit's C-terminal domain are mutually exclusive. *Biochimica et biophysica acta. Bioenergetics* **2020,** *1861* (7), 148189; (b) Kuhlbrandt, W., Structure and Mechanisms of F-Type ATP Synthases. *Annu Rev Biochem* **2019,** *88*, 515-549.
15. Hards, K.; McMillan, D. G. G.; Schurig-Briccio, L. A.; Gennis, R. B.; Lill, H.; Bald, D.; Cook, G. M., Ionophoric effects of the antitubercular drug bedaquiline. *Proceedings of the National Academy of Sciences of the United States of America* **2018,** *115* (28), 7326-7331.
16. Moerner, W. E.; Kador, L., Optical detection and spectroscopy of single molecules in a solid. *Physical review letters* **1989,** *62* (21), 2535-2538.
17. Xue, Q.; Yeung, E. S., Differences in the chemical reactivity of individual molecules of an enzyme. *Nature* **1995,** *373* (6516), 681-3.
18. Lu, H. P.; Xun, L.; Xie, X. S., Single-molecule enzymatic dynamics. *Science* **1998,** *282* (5395), 1877-82.
19. Xie, X. S.; Lu, H. P., Single-molecule enzymology. *The Journal of biological chemistry* **1999,** *274* (23), 15967-70.
20. (a) Craig, D. B.; Arriaga, E. A.; Wong, J. C. Y.; Lu, H.; Dovichi, N. J., Studies on single alkaline phosphatase molecules: Reaction rate and activation energy of a reaction catalyzed by a single molecule and the effect of thermal denaturation - The death of an enzyme. *Journal of the American Chemical Society* **1996,** *118* (22), 5245-5253; (b) Polakowski, R.; Craig, D. B.; Skelley, A.; Dovichi, N. J., Single molecules of highly purified bacterial alkaline phosphatase have identical activity. *Journal of the American Chemical Society* **2000,** *122* (20), 4853-4855.
21. Ha, T.; Enderle, T.; Ogletree, D. F.; Chemla, D. S.; Selvin, P. R.; Weiss, S., Probing the interaction between two single molecules: Fluorescence resonance energy transfer between a single donor and a single acceptor. *Proceedings of the National Academy of Sciences of the United States of America* **1996,** *93* (13), 6264-6268.
22. Lerner, E.; Cordes, T.; Ingargiola, A.; Alhadid, Y.; Chung, S.; Michalet, X.; Weiss, S., Toward dynamic structural biology: Two decades of single-molecule Forster resonance energy transfer. *Science* **2018,** *359* (6373), 288-+.
23. Hellenkamp, B.; Schmid, S.; Doroshenko, O.; Opanasyuk, O.; Kuhnemuth, R.; Rezaei Adariani, S.; Ambrose, B.; Aznauryan, M.; Barth, A.; Birkedal, V.; Bowen, M. E.; Chen, H.; Cordes, T.; Eilert, T.; Fijen, C.; Gebhardt, C.; Gotz, M.; Gouridis, G.; Gratton, E.; Ha, T.; Hao, P.; Hanke, C. A.; Hartmann, A.; Hendrix, J.; Hildebrandt, L. L.; Hirschfeld, V.; Hohlbein, J.; Hua, B.;

Hubner, C. G.; Kallis, E.; Kapanidis, A. N.; Kim, J. Y.; Krainer, G.; Lamb, D. C.; Lee, N. K.; Lemke, E. A.; Levesque, B.; Levitus, M.; McCann, J. J.; Naredi-Rainer, N.; Nettels, D.; Ngo, T.; Qiu, R.; Robb, N. C.; Rocker, C.; Sanabria, H.; Schlierf, M.; Schroder, T.; Schuler, B.; Seidel, H.; Streit, L.; Thurn, J.; Tinnefeld, P.; Tyagi, S.; Vandenberk, N.; Vera, A. M.; Weninger, K. R.; Wunsch, B.; Yanez-Orozco, I. S.; Michaelis, J.; Seidel, C. A. M.; Craggs, T. D.; Hugel, T., Precision and accuracy of single-molecule FRET measurements-a multi-laboratory benchmark study. *Nature methods* **2018,** *15* (9), 669-676.

24. Boyer, P. D., The ATP synthase--a splendid molecular machine. *Annu Rev Biochem* **1997,** *66*, 717-49.

25. Abrahams, J. P.; Leslie, A. G.; Lutter, R.; Walker, J. E., Structure at 2.8 A resolution of F1-ATPase from bovine heart mitochondria. *Nature* **1994,** *370* (6491), 621-8.

26. Duncan, T. M.; Bulygin, V. V.; Zhou, Y.; Hutcheon, M. L.; Cross, R. L., Rotation of subunits during catalysis by Escherichia coli F1-ATPase. *Proceedings of the National Academy of Sciences of the United States of America* **1995,** *92* (24), 10964-8.

27. Sabbert, D.; Engelbrecht, S.; Junge, W., Intersubunit rotation in active F-ATPase. *Nature* **1996,** *381* (6583), 623-5.

28. Noji, H.; Yasuda, R.; Yoshida, M.; Kinosita, K., Jr., Direct observation of the rotation of F1-ATPase. *Nature* **1997,** *386* (6622), 299-302.

29. (a) Yoshida, M.; Muneyuki, E.; Hisabori, T., ATP synthase - a marvellous rotary engine of the cell. *Nat Rev Mol Cell Biol* **2001,** *2* (9), 669-77; (b) Watanabe, R.; Genda, M.; Kato-Yamada, Y.; Noji, H., Essential Role of the epsilon Subunit for Reversible Chemo-Mechanical Coupling in F1-ATPase. *Biophysical journal* **2018,** *114* (1), 178-187.

30. Nakanishi-Matsui, M.; Kashiwagi, S.; Hosokawa, H.; Cipriano, D. J.; Dunn, S. D.; Wada, Y.; Futai, M., Stochastic high-speed rotation of Escherichia coli ATP synthase F1 sector: the epsilon subunit-sensitive rotation. *The Journal of biological chemistry* **2006,** *281* (7), 4126-31.

31. Suzuki, T.; Tanaka, K.; Wakabayashi, C.; Saita, E.; Yoshida, M., Chemomechanical coupling of human mitochondrial F1-ATPase motor. *Nature chemical biology* **2014,** *10* (11), 930-6.

32. (a) Kobayashi, R.; Ueno, H.; Li, C. B.; Noji, H., Rotary catalysis of bovine mitochondrial F1-ATPase studied by single-molecule experiments. *Proceedings of the National Academy of Sciences of the United States of America* **2020,** *117* (3), 1447-1456; (b) Zarco-Zavala, M.; Watanabe, R.; McMillan, D. G. G.; Suzuki, T.; Ueno, H.; Mendoza-Hoffmann, F.; Garcia-Trejo, J. J.; Noji, H., The 3 x 120 degrees rotary mechanism of Paracoccus denitrificans F1-ATPase is different from that of the bacterial and mitochondrial F1-ATPases. *Proceedings of the National Academy of Sciences of the United States of America* **2020,** *117* (47), 29647-29657.

33. (a) Sambongi, Y.; Iko, Y.; Tanabe, M.; Omote, H.; Iwamoto-Kihara, A.; Ueda, I.; Yanagida, T.; Wada, Y.; Futai, M., Mechanical rotation of the c subunit oligomer in ATP synthase (F0F1): direct observation. *Science* **1999,** *286* (5445), 1722-4; (b) Kaim, G.; Prummer, M.; Sick, B.; Zumofen, G.; Renn, A.; Wild, U. P.; Dimroth, P., Coupled rotation within single F0F1 enzyme complexes during ATP synthesis or hydrolysis. *FEBS letters* **2002,** *525* (1-3), 156-63.

34. Borsch, M.; Diez, M.; Zimmermann, B.; Reuter, R.; Graber, P., Stepwise rotation of the gamma-subunit of EF(0)F(1)-ATP synthase observed by intramolecular single-molecule fluorescence resonance energy transfer. *FEBS letters* **2002,** *527* (1-3), 147-52.

35. (a) Diez, M.; Zimmermann, B.; Borsch, M.; Konig, M.; Schweinberger, E.; Steigmiller, S.; Reuter, R.; Felekyan, S.; Kudryavtsev, V.; Seidel, C. A.; Graber, P., Proton-powered subunit rotation in single membrane-bound FoF1-ATP synthase. *Nature structural & molecular biology* **2004,** *11* (2), 135-41; (b) Zimmermann, B.; Diez, M.; Zarrabi, N.; Graber, P.; Borsch, M.,

Movements of the epsilon-subunit during catalysis and activation in single membrane-bound H(+)-ATP synthase. *The EMBO journal* **2005,** *24* (12), 2053-63; (c) Duser, M. G.; Zarrabi, N.; Cipriano, D. J.; Ernst, S.; Glick, G. D.; Dunn, S. D.; Borsch, M., 36 degrees step size of proton-driven c-ring rotation in FoF1-ATP synthase. *The EMBO journal* **2009,** *28* (18), 2689-2696.

36. Sielaff, H.; Yanagisawa, S.; Frasch, W. D.; Junge, W.; Borsch, M., Structural Asymmetry and Kinetic Limping of Single Rotary F-ATP Synthases. *Molecules* **2019,** *24*, 504.

37. (a) Cohen, A. E.; Moerner, W. E., Method for trapping and manipulating nanoscale objects in solution. *Appl. Phys. Lett.* **2005,** *86*, 093109; (b) Cohen, A. E.; Moerner, W. E., The anti-Brownian electrophoretic trap (ABEL trap): fabrication and software. *Proc. SPIE* **2005,** *5699*, 296-305; (c) Cohen, A. E.; Moerner, W. E., Controlling Brownian motion of single protein molecules and single fluorophores in aqueous buffer. *Optics express* **2008,** *16* (10), 6941-56; (d) Fields, A. P.; Cohen, A. E., Electrokinetic trapping at the one nanometer limit. *Proceedings of the National Academy of Sciences of the United States of America* **2011,** *108* (22), 8937-42; (e) Wang, Q.; Moerner, W. E., Optimal strategy for trapping single fluorescent molecules in solution using the ABEL trap. *Appl Phys B* **2010,** *99* (1-2), 23-30.

38. (a) Heitkamp, T.; Deckers-Hebestreit, G.; Börsch, M., Observing single FoF1-ATP synthase at work using an improved fluorescent protein mNeonGreen as FRET donor. *Proc. SPIE* **2016,** *9714*, 97140B; (b) Weiss, M.; Frohnmayer, J. P.; Benk, L. T.; Haller, B.; Janiesch, J. W.; Heitkamp, T.; Borsch, M.; Lira, R. B.; Dimova, R.; Lipowsky, R.; Bodenschatz, E.; Baret, J. C.; Vidakovic-Koch, T.; Sundmacher, K.; Platzman, I.; Spatz, J. P., Sequential bottom-up assembly of mechanically stabilized synthetic cells by microfluidics. *Nat Mater* **2018,** *17* (1), 89-96.

39. Duser, M. G.; Bi, Y.; Zarrabi, N.; Dunn, S. D.; Borsch, M., The proton-translocating a subunit of F0F1-ATP synthase is allocated asymmetrically to the peripheral stalk. *The Journal of biological chemistry* **2008,** *283* (48), 33602-10.

40. Sobti, M.; Walshe, J. L.; Wu, D.; Ishmukhametov, R.; Zeng, Y. C.; Robinson, C. V.; Berry, R. M.; Stewart, A. G., Cryo-EM structures provide insight into how E. coli F1Fo ATP synthase accommodates symmetry mismatch. *Nature communications* **2020,** *11* (1), 2615.

41. Borsch, M., Single-molecule fluorescence resonance energy transfer techniques on rotary ATP synthases. *Biological chemistry* **2011,** *392* (1-2), 135-142.

42. Dathe, A.; Heitkamp, T.; Pérez, I.; Sielaff, H.; Westphal, A.; Reuter, S.; Mrowka, R.; Börsch, M., Observing monomer - dimer transitions of neurotensin receptors 1 in single SMALPs by homoFRET and in an ABELtrap. *Proc. SPIE* **2019,** *10884*, 108840N.

43. Rendler, T.; Renz, M.; Hammann, E.; Ernst, S.; Zarrabi, N.; Borsch, M., Monitoring single membrane protein dynamics in a liposome manipulated in solution by the ABELtrap. *Proc. SPIE* **2011,** *7902*, 79020M.

44. Zarrabi, N.; Zimmermann, B.; Diez, M.; Graber, P.; Wrachtrup, J.; Borsch, M., Asymmetry of rotational catalysis of single membrane-bound F0F1-ATP synthase. *Proc. SPIE* **2005,** *5699*, 175-188.

45. Su, B.; Duser, M. G.; Zarrabi, N.; Heitkamp, T.; Starke, I.; Borsch, M., Observing conformations of single FoF1-ATP synthases in a fast anti-Brownian electrokinetic trap. *Proc. SPIE* **2015,** *9329*, 93290A.

46. Ploetz, E.; Lerner, E.; Husada, F.; Roelfs, M.; Chung, S.; Hohlbein, J.; Weiss, S.; Cordes, T., Forster resonance energy transfer and protein-induced fluorescence enhancement as synergetic multi-scale molecular rulers. *Sci Rep* **2016,** *6*, 33257.

47. Vandenberk, N.; Barth, A.; Borrenberghs, D.; Hofkens, J.; Hendrix, J., Evaluation of Blue and Far-Red Dye Pairs in Single-Molecule Forster Resonance Energy Transfer Experiments. *The journal of physical chemistry. B* **2018,** *122* (15), 4249-4266.

48. Rasnik, I.; McKinney, S. A.; Ha, T., Nonblinking and long-lasting single-molecule fluorescence imaging. *Nature methods* **2006,** *3* (11), 891-3.
49. Hanes, C. S., Studies on plant amylases: The effect of starch concentration upon the velocity of hydrolysis by the amylase of germinated barley. *The Biochemical journal* **1932,** *26* (5), 1406-21.
50. Lineweaver, H.; Burk, D., The Determination of Enzyme Dissociation Constants. *J. Am. Chem. Soc.* **1934,** *56* (3), 658–666.
51. Oka, H.; Hosokawa, H.; Nakanishi-Matsui, M.; Dunn, S. D.; Futai, M.; Iwamoto-Kihara, A., Elastic rotation of Escherichia coli FOF1 having ε subunit fused with cytochrome b562 or flavodoxin reductase. *Biochemical and biophysical research communications* **2014,** *446* (4), 889-893.
52. Peskova, Y. B.; Nakamoto, R. K., Catalytic control and coupling efficiency of the Escherichia coli FoF1 ATP synthase: influence of the Fo sector and epsilon subunit on the catalytic transition state. *Biochemistry* **2000,** *39* (38), 11830-6.
53. Lobau, S.; Weber, J.; Senior, A. E., Catalytic site nucleotide binding and hydrolysis in F1F0-ATP synthase. *Biochemistry* **1998,** *37* (30), 10846-53.
54. Ishmukhametov, R. R.; Galkin, M. A.; Vik, S. B., Ultrafast purification and reconstitution of His-tagged cysteine-less Escherichia coli F1Fo ATP synthase. *Biochimica et biophysica acta* **2005,** *1706* (1-2), 110-6.
55. Johnson, K. M.; Swenson, L.; Opiparl, A. W.; Reuter, R.; Zarrabi, N.; Fierke, C. A.; Borsch, M.; Glick, G. D., Mechanistic Basis for Differential Inhibition of the F1F0-ATPase by Aurovertin. *Biopolymers* **2009,** *91* (10), 830-840.
56. Bilyard, T.; Nakanishi-Matsui, M.; Steel, B. C.; Pilizota, T.; Nord, A. L.; Hosokawa, H.; Futai, M.; Berry, R. M., High-resolution single-molecule characterization of the enzymatic states in Escherichia coli F1-ATPase. *Philosophical transactions of the Royal Society of London. Series B, Biological sciences* **2013,** *368* (1611), 20120023.
57. Cingolani, G.; Duncan, T. M., Structure of the ATP synthase catalytic complex (F(1)) from Escherichia coli in an autoinhibited conformation. *Nature structural & molecular biology* **2011,** *18* (6), 701-7.
58. Wilkens, S.; Capaldi, R. A., Solution structure of the ε subunit of the F_1-ATPase from *Escherichia coli* and interactions of this subunit with β subunits in the complex. *Journal of Biological Chemistry* **1998,** *273* (41), 26645-26651.
59. (a) Duncan, T. M.; Duser, M. G.; Heitkamp, T.; McMillan, D. G.; Borsch, M., Regulatory conformational changes of the epsilon subunit in single FRET-labeled FoF1-ATP synthase. *Proc. SPIE* **2014,** *8948*, 89481J; (b) Sobti, M.; Ishmukhametov, R.; Bouwer, J. C.; Ayer, A.; Suarna, C.; Smith, N. J.; Christie, M.; Stocker, R.; Duncan, T. M.; Stewart, A. G., Cryo-EM reveals distinct conformations of E. coli ATP synthase on exposure to ATP. *eLife* **2019,** *8*; (c) Bockenhauer, S. D.; Duncan, T. M.; Moerner, W. E.; Borsch, M., The regulatory switch of F1-ATPase studied by single-molecule FRET in the ABEL Trap. *Proc. SPIE* **2014,** *8950*, 89500H; (d) Rodgers, A. J.; Wilce, M. C., Structure of the γ-ε complex of ATP synthase. *Nat. Struct. Biol.* **2000,** *7* (11), 1051-1054.
60. Sobti, M.; Walshe, J. L.; Zeng, Y. C.; Ishmukhametov, R.; Stewart, A. G., Subunit epsilon of E. coli F1Fo ATP synthase attenuates enzyme activity by modulating central stalk flexibility. BioRxiv, 2020.

Supporting Information

Fast ATP-dependent subunit rotation in reconstituted F_oF_1-ATP synthase trapped in solution

Thomas Heitkamp, Michael Börsch

Single-Molecule Microscopy Group, Jena University Hospital, D-07743 Jena, Germany.

Email: michael.boersch@med.uni-jena.de

Phone +49 3641 9396618, Fax +49 3641 9396621

Content: preparation of FRET-labeled F_oF_1-ATP synthase from *E. coli* including fluorophore labeling, reconstitution, catalytic activity measurements of ATP hydrolysis and synthesis, the confocal ABEL trap setup, PDMS/glass sample chamber preparation, photophysics of FRET fluorophores bound to the enzyme with and without the antioxidant "*trolox*", photon bursts of single FRET-labeled F_oF_1-ATP synthases in the presence of 100 µM ATP, 40 µM ATP, 20 µM ATP and 5 µM ATP, distributions of fluctuating FRET level durations, Lineweaver-Burk analysis of smFRET-based ATP hydrolysis rates.

1. Preparation of FRET-labeled F_oF_1-ATP synthase reconstituted in liposomes

1.1 Plasmids and *E. coli* expression strain. To achieve specific labeling at defined cysteine positions within the F_o part and the F_1 part of F_oF_1-ATP synthase, the two parts had to be purified and labeled separately as developed previously [1]. Here, after reconstituting F_oF_1-ATP synthase labeled at the a-subunit into liposomes, its unlabeled F_1 part was stripped and replaced by the labeled F_1 part to yield the FRET-labeled reconstituted enzyme. F_oF_1-ATP synthase carrying a cysteine at the extended C-terminus of the a-subunit (a-GAACA, F_o-(a-SH)F_1-ATP synthase in the following) and the F_1 parts carrying the H56C substitution in the ε-subunit were produced using the corresponding plasmids pMB14 (a-GAACA) [2] and pRAP100 (εH56C) [3] which are derivatives of pRA100 [4]. Plasmids were transformed into *Escherichia coli* strain RA1 (*F- thi rpsL gal Δ(cyoABCDE) 456::KAN Δ(atpB-atpC)ilv:Tn10*) [5], and cells were grown in a 10-L fermenter [6].

1.2. Purification of F_o-(a-SH)F_1-ATP synthase. Tag-free F_o-(a-SH)F_1-ATP synthase was purified using three chromatography steps [6]. In brief, F_oF_1-containing membranes were isolated, washed to remove membrane-associated proteins and solubilized with n-dodecyl β-D-maltoside (DDM) as detergent (SDS-PAGE shown in Figure S1 below, lane "Mem"). Ultracentrifugation was applied to remove non-solubilized material. Solubilized membrane proteins (Figure S1, lane "Sol") were concentrated by ammonium sulfate precipitation and separated from lipids, nucleotides and salts by size exclusion chromatography (SEC) using a self-packed XK26/60 Sephacryl S-300 column. The eluted protein fractions (Figure S1, lane "1. SEC") were loaded separately onto an anion exchange (IEX) column Poros HQ 20 (4.6 x 100 mm, Applied Biosystems, USA). The F_OF_1-containing peak fractions were pooled (Figure S1, lane "IEX"), concentrated by ammonium sulfate precipitation and loaded onto a Tricorn Superose 6 10/300 GL size exclusion column (GE Healthcare, USA) for refinement. The second SEC was mainly used for desalting and for separation of dissociated F_o and F_1 fractions. The protein fractions containing intact, pure F_oF_1 with all subunits (Figure S1, lane "2. SEC") were separately shock-frozen in liquid nitrogen and stored at -80°C for subsequent labeling.

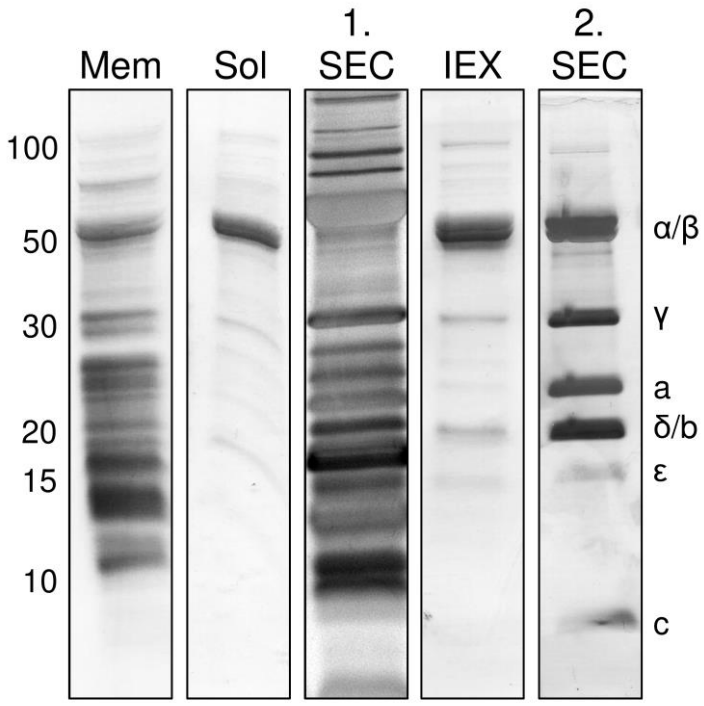

Figure S1. SDS-PAGE of the F_o-(a-SH)F_1-ATP synthase purification steps from *E. coli* membranes. Acrylamide concentration was 12 %, staining with coomassie-R250. Molecular weight numbers in kDa on the left, F_oF_1 subunit assignment on the right.

1.3. Purification of F_1-(εH56C) parts. Tag-free F_1-(εH56C) parts were purified using established protocols [3, 7] with minor modifications. Briefly, F_oF_1-containing membranes were isolated and washed with low ionic strength buffers (SDS-PAGE shown in Figure S2 below, lane "Mem"). The soluble F_1 part was then stripped from the membrane-embedded F_o part using buffer without $MgCl_2$ and 4-aminobenzamidine. This fraction (Figure S2, lane "Strip") was loaded on a self-packed Poros HQ 20 (10 x 200 mm) anion exchange column (Applied Biosystems, USA). The F_1 parts were almost pure (Figure S2, lane "IEX"). Only two impurities between 12 and 20 kDa and some faint protein bands in the high molecular range were were remaining. Therefore, F1 parts were concentrated by ammonium sulfate precipitation and loaded on a Tricorn Superose 6 10/300 GL column (GE Healthcare, USA) for size exclusion chromatography. The major protein peak fractions containing F_1 parts (Figure S2, lane "SEC") were pooled, concentrated using an Amicon Ultra-15 Ultracell 30K (Merck Millipore, USA), shock-frozen in liquid nitrogen and stored at -80 °C.

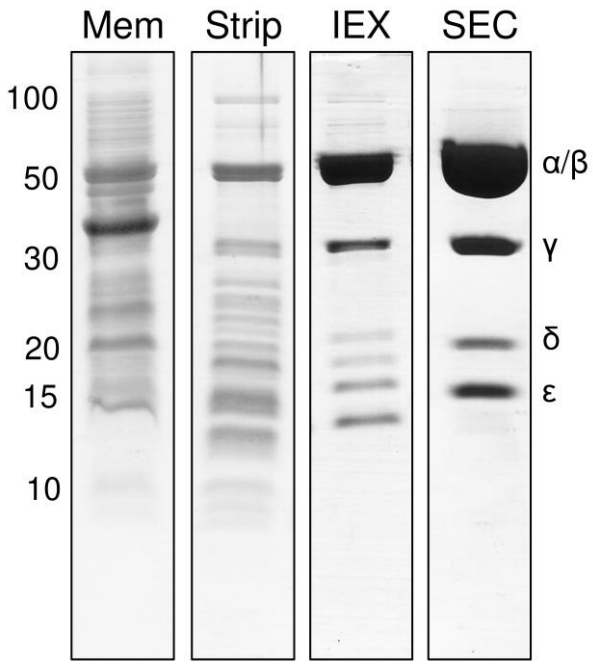

Figure S2. SDS-PAGE of F_1-(εH56C) part purification steps from *E. coli* membranes. Acrylamide concentration was 12 %, staining with coomassie-R250. Molecular weight numbers in kDa on the left, F_1 subunit assignment on the right.

1.4. Fluorescence labeling of the a- and ε-subunit. Cysteine labeling reactions were carried out as described [3, 6]. Purified F_o-(a-SH)F_1-ATP synthase or purified F_1-(εH56C) were first concentrated by precipitation with $(NH_4)_2SO_4$, dissolved in 75 µl 50 mM MOPS-NaOH pH 7.0, with 0.1 mM $MgCl_2$ and, in the case of F_oF_1, with 0.1 % DDM ("labeling buffer with DDM"). The resolved proteins were desalted by size exclusion chromatography using 1 ml columns filled with Sephadex G50 medium (GE Healthcare, USA), equilibrated by gravity flow with labeling buffer and pre-spinned for 2 min with 250 × g at room temperature. The resolved proteins were then eluted by centrifugation for 2.5 min at 445 × g. Concentrations of the desalted enzymes were calculated by absorption measurements at 280 nm (Lambda 650, PerkinElmer, USA) using a molar extinction coefficient (ε_{280nm}) of 303,130 $L \cdot mol^{-1} \cdot cm^{-1}$ for F_oF_1 and 206,060 $L \cdot mol^{-1} \cdot cm^{-1}$ for F_1.

The cysteine in the a-subunit of F_oF_1 was labeled with Alexa Fluor 647 C_2-maleimide (Thermo Fischer Scientific Inc., USA) and the cysteine in the ε subunit of F_1 was labeled with Cy3B maleimide (GE Healthcare, USA). Labeling was carried out in labeling buffer with a five-fold molar excess of Tris(2-carboxyethyl)phosphine (TCEP) to protein on ice, in a total volume of 100 µl using a protein concentration of 10 µM F_oF_1 or 14 µM F_1 and a 1:1.1 stoichiometric ratio of

enzyme to dye. Reactions were stopped after 15 minutes by three consecutive Sephadex G50 medium spin columns. Labeling efficiencies were determined by comparing absorption at 280 nm and dye absorption at its maximum (Cy3B: ε_{559nm} = 130,000 L·mol^{-1}·cm^{-1}; Alexa Fluor 647: ε_{654nm} = 265,000 L·mol^{-1}·cm^{-1}). Shown in Figure S3, labeling the ε-subunit with Cy3B-maleimide was achieved with an efficiency of 73.7 %. Labeling efficiency of the a-subunit with Alexa Fluor 647-maleimide was 31.9 %. We noticed that the spectrum of enzyme-bound Alexa Fluor 647 was shifted about 7 nm towards longer wavelengths.

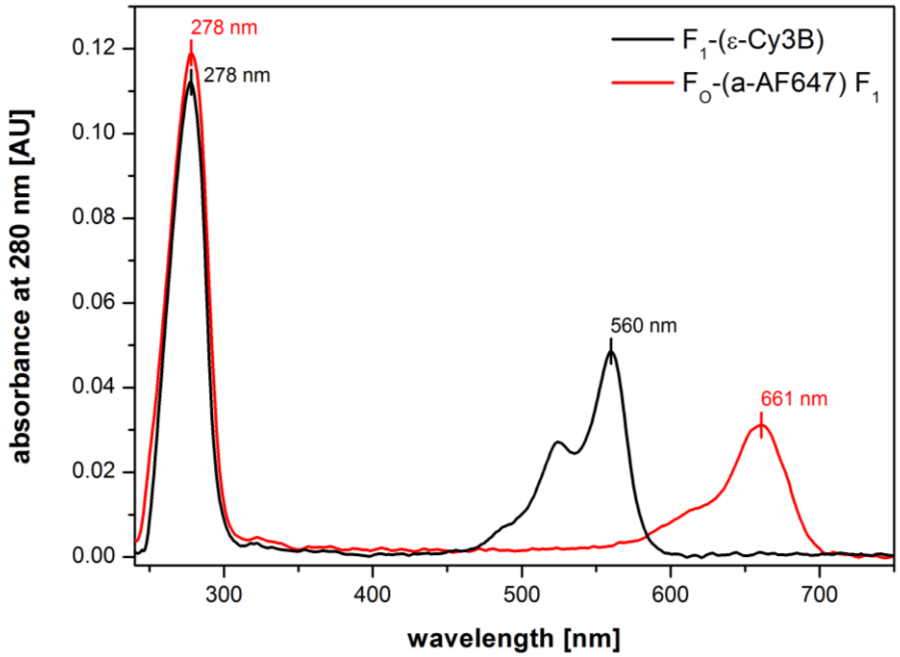

Figure S3. Absorbance spectra of Cy3B-labeled F_1-(εH56C) parts (black curve) and of Alexa Fluor 647-labeled F_o-(a-SH)F_1-ATP synthase (red curve).

Labeling specificity was checked by SDS-PAGE with subsequent fluorography (Figure S4). Labeling with both dyes were highly specific. The labeled proteins were adjusted with 10 % (v/v) glycerol in buffer, flash frozen as 5 µl aliquots in liquid N_2 and stored at -80°C.

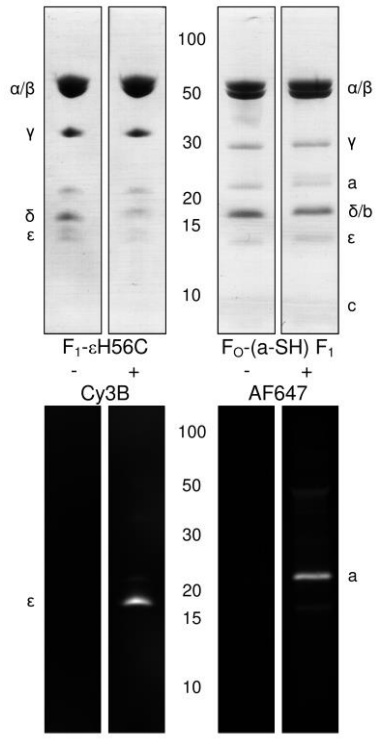

Figure S4. SDS-PAGE of F_1-(εH56C) parts and of F_o-(a-SH)F_1-ATP synthase before (-) and after (+) labeling with Cy3B or Alexa Fluor 647, respectively. Upper panels are white-light transmission images of gels stained with coomassie-R250. Lower panels are fluorescence images showing the specificity of the labeling.

1.5. Reconstitution of F_oF_1-ATP synthase and exchange of F_1 parts to yield FRET-labeled F_oF_1-ATP synthase in liposomes. First, Alexa Fluor 647-labeled F_oF_1-ATP synthase was reconstituted into pre-formed liposomes [6]. Liposomes were generated by evaporating chloroform solutions of phosphatidylcholine (Lipoid GmbH, Germany) and phosphatidic acid (Sigma-Aldrich, Germany) in a mass ratio of 19:1. The dried lipid film was resolved to 18 g/l in 10 mM Tricine-NaOH pH 8.0, 0.1 mM EDTA, 0.5 mM DTT, 7.2 g/l cholic acid and 3.6 g/l desoxycholate. The suspension was sonicated and dialyzed at 30°C for 5 h against the 4,000-fold volume of 10 mM Tricine-NaOH pH 8.0, 0.2 mM EDTA, 0.25 mM DTT and 2.5 mM $MgCl_2$. In a total volume of 1.2 ml, 200 µl of these pre-formed liposomes, 2.5 mM $MgCl_2$, "reconstitution buffer" (20 mM Tricine-NaOH pH 8.0, 20 mM succinate, 50 mM NaCl and 0.6 mM KCl), 20 nM labeled F_oF_1 and 0.8% (v/v) Triton-X-100 were mixed in exactly this order under vigorous shaking. After 1 h incubation with gentle shaking, 128 mg of pre-treated BioBeads SM-2 (Biorad, USA) were added to remove the detergent. After 1 hour, the proteoliposomes were separated from the BioBeads.

Second, the unlabeled F_1 part was removed from reconstituted F_oF_1 as described [8]. Liposomes were diluted three times 25-fold with a low ionic strength buffer (1 mM Tricine–NaOH pH 8.0, 1 mM DTT, 0.5 mM EDTA, and 4% (v/v) glycerol) without $MgCl_2$, incubated for 1 h at room temperature and centrifuged at 300,000 × g for 1.5 h at room temperature. The remaining F_o-liposomes were resuspended in the buffer above with 10% glycerol to yield a F_o concentration of 125-150 nM and stored overnight in the dark.

Third, rebinding of Cy3B-labeled F_1 to F_o-liposomes was achieved as described [8]. The Alexa Fluor 647-F_o-liposome suspension was incubated with Cy3B-labeled F_1 in solution at a molar excess of three F_1 per F_O in the presence of 2.5 mM $MgCl_2$ and 50 mM NaCl for 45 min at 37°C, followed by 90 min incubation at 0°C. Unbound F_1 was removed by two ultracentrifugation runs (90 min, 300,000 × g, 4°C), each time resuspending pelleted proteoliposomes in 20 mM Tricine-NaOH (pH 8.0), 20 mM succinic acid, 50 mM NaCl, 0.6 mM KCl, 2.5 mM $MgCl_2$ and 4% (v/v) glycerol. The proteoliposomes were adjusted to 10% (v/v) glycerol, flash-frozen as 5 µl aliquots in liquid nitrogen and stored at −80°C. The final concentration of FRET-labeled F_oF_1 in proteoliposomes was estimated to ~40 nM.

1.6. Measurement of ATP hydrolysis rates. ATP hydrolysis was measured using a continuous coupled enzymatic assay [6, 9]. Solubilized enzyme (3-10 nM) was added to the 37°C pre-warmed reaction buffer (100 mM Tris-HCl pH 8.0, 25 mM KCl, 4 mM MgCl2, 2.5 mM phosphoenolpyruvate, 18 units/ml pyruvate kinase, 16 units/ml lactate dehydrogenase, 2 mM ATP and 0.4 mM NADH), and ATP hydrolysis was followed by the decrease of NADH absorbance. The ATP hydrolysis rate was calculated from the linear slope using an extinction coefficient of 6,220 L mol^{-1} cm^{-1} for NADH. By adding N,N-dimethyl-n-dodecylamine N-oxide (LDAO) to a final concentration of 0.6 % (v/v), possible activation of the enzyme as an indicator for purification quality was verified [10]. Solubilized F_oF_1 in detergent showed significantly lower ATP hydrolysis rates than F_1 (Figure S5). However, LDAO-induced activation of F_oF_1 was in good agreement with reported values. Labeling with fluorescent dyes had no significant effect on ATP hydrolysis activities of the enzyme mutants.

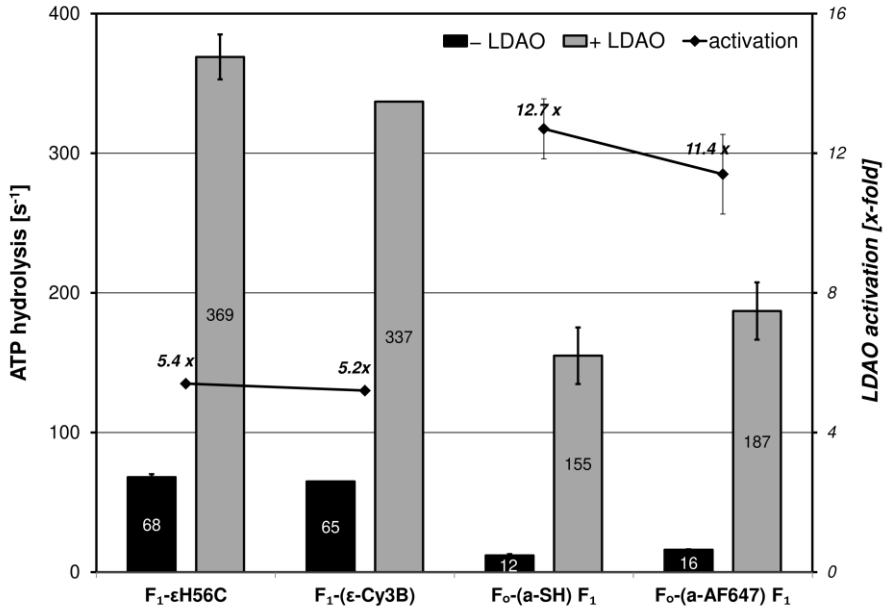

Figure S5. ATP hydrolysis rates of F_1-(εH56C) parts and DDM-solubilized F_o-(a-SH)F_1-ATP synthase before and after fluorescence labeling.

1.7. Measurement of ATP synthesis rates. ATP synthesis rates were determined as described [11] using the luciferin/luciferase luminescence assay. The cysteine mutation at the C-terminus of the a-subunit and fluorophore labeling did not affect ATP synthesis activity of reconstituted F_oF_1-ATP synthase compared to the "wildtype" enzyme (Figure S6). However, after rebinding F_1 to F_o-liposomes the FRET-labeled enzyme showed less than half of the ATP synthesis activity. This was likely a F_oF_1 concentration artefact due to the loss of proteoliposomes during each of the ultracentrifugation steps and had been discussed previously [3, 9b]. Therefore, a mean ATP synthesis rate 16±2 ATP*s^{-1} for the reassembled FRET-labeled enzyme is in good agreement either with previously reported 21±4 ATP*s^{-1} for a similar FRET-labeled F_oF_1-ATP synthase comprising the same cysteine mutation εH56C in F_1, cysteine mutation in the b-subunits, and rebinding of F_1 to F_o procedures [3], or with a ATP synthesis rate of 32±7 ATP*s^{-1} for F_oF_1 with EGFP (or mNeonGreen, respectively) fused to the C-terminus of the a-subunit but without rebinding F_1 [6, 12].

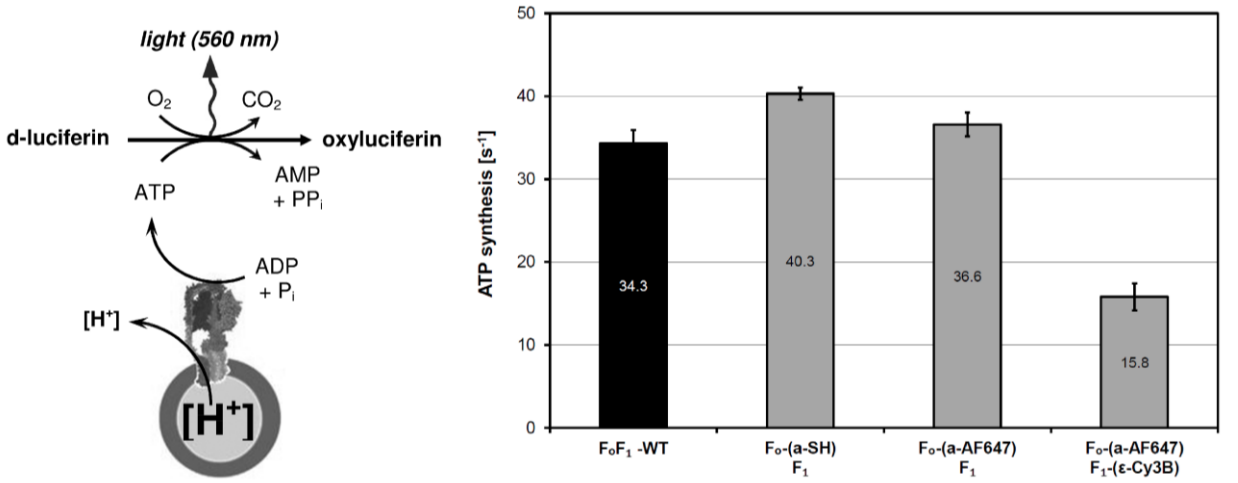

Figure S6. Principle of the luciferin/luciferase assay for ATP synthesis measurements (left). Comparison of ATP synthesis rates of F_o-(a-SH)F_1-ATP synthase before and after labeling with Alexa Fluor 647, "wild-type" F_oF_1 and the reassembled FRET-labeled F_oF_1-ATP synthase.

2. The confocal ABEL trap setup

2.1. Confocal setup. We have built different ABEL traps with APD detectors using a variety of lasers and associated optical filter sets [13]. Here, the beam diameter of a continuous-wave 532 nm laser (Compass 315M, Coherent) was collimated and adjusted to less than 1 mm by a two lens telescope, and linearly polarized by a polarizing beam splitter cube [14]. Laser power was set to 40 µM using a variable metallic neutral density filter. Beam steering was achieved by two consecutive electro-optical deflectors (M310A, Conoptics) with an achromatic λ/2 wave plate in between, each powered by fast high-voltage amplifier (7602 M, Krohn-Hite) and controlled by the field-programmable gate array (FPGA card PCIe-7852R, National Instruments). The FPGA LabView software to run the ABEL trap [15] was used with minor modifications to implement the 32-point knight pattern in the focus plane [16] and to extend the number of trapping channels up to four.

Entering the inverted microscope (IX 71, Olympus) *via* the epifluorescence port, the laser beam was directed to a 60x oil immersion objective with n.a. 1.42 (PlanAPO, Olympus) using a dichroic mirror (z 532 RD, F43-537, AHF). From the focal plane, fluorescence was focused to a 300 µm pinhole by the tube lens on the left side port of the IX71 and separated into two spectral channels by a dichroic beam splitter at 640 nm (zt 640 RDC, F48-640, AHF). FRET donor Cy3B photons were detected in the range between 545 nm and 620 nm (582/75 BrightLine HC, F37-582, AHF),

and FRET acceptor Alexa Fluor 647 photons for wavelengths $\lambda > 647$ nm (Raman RazorEdge LP 647 RU, F76-647, AHF). Given filter specifications and available fluorescence spectra at *www.FPbase.org*, the filter-based spectral detection efficiency for Cy3B was estimated to 69.2 % in the FRET donor channel plus a spectral crosstalk of 11.4 % into the acceptor channel. Alexa Fluor 647 was detected in the acceptor channel with 92.3 % efficiency and without a crosstalk to the donor channel. Time-correlated single photon counting (TCSPC) by two avalanche photodiode detectors (SPCM AQRH-14, Excelitas) was achieved with 164 ps time resolution using the TCSPC inputs of the counter electronics (DPC 230 Becker&Hickl) and an external sync signal. Both APDs were mounted on a single 3D-adjustable mechanical stage system (home-built with components from OWIS) that also contained the pinhole. Positioning of the ABEL trap chip on the microscope was possible using a mechanical stage (x, y translation with µm resolution) and the z-positioner of the IX71, plus an 3D piezo scanner (P-527.3CD, Physik Instrumente) with sub-nm resolution mounted on top of the mechanical stage.

2.2. FPGA-based ABEL trap. The multiplexed APD signals were counted in parallel by the FPGA card in a separate measurement computer. A Kalman filter in the FPGA software correlated the APD signals with respect to the actual laser focus in the knight tour pattern to estimate the position of the fluorescent particle and to generate the feedback voltages to the four Pt-electrodes. The voltage amplifier limit was set to ±10V at the electrodes. This version of the FPGA LabView software required optimization of several parameter settings to trap the negatively-charged proteoliposomes for long times: for the 32-point knight pattern in a 6 x 6 array, the distance between the focus position was 0.47 µm, the repetition rate of the full pattern was either 5 or 7 kHz, the dimensions of the pattern in the focal plane were 2.34 x 2.34 µm, the waist of the laser focus was estimated to 0.6 µm using 100-nm-tetraspeck bead scanning of immobilized beads, and the EOD deflection scale was 0.117 µm/V. The values for the estimated diffusion constant in the software in order to trap proteoliposomes was set to 5 $\mu m^2/s$, and the estimated electric mobility was set to -80 µm/s/V.

Trapping of FRET-labeled F_oF_1-ATP synthases was achieved using the combined photon counts from donor and acceptor channel. Qualitatively, "good trapping" of proteoliposomes was classified by online monitoring of three indicators simultaneously as shown in three panels of the graphical user interface: (1) maximum brightness (i.e. combined donor and acceptor photon count rates) and minimal intensity fluctuations of a trapped particle, (2) the generated feedback voltages (symmetric

for ±x and ±y voltages, low voltage fluctuating around 0 V during trapping in solution) and (3) the visualized trapping position within the center (0,0 position) of knight tour pattern. The quality of the PDMS/glass sample chamber (i.e. the symmetry of the thin channels in the cross-like trapping region, see below) and the embedding of the electrodes in the sample buffer could be assessed. Furthermore, proteoliposomes which were temporarily attached to the surface, could be revealed in real time. Brightness loss in combination with shorter trapping durations also indicated a z-drift of the sample chamber with respect to the focal plane and prompted manual adjustment of the z-position by quick refocusing using the ocular port of the microscope.

2.3. PDMS/glass chips. The custom-made wafer used to mold the PDMS part of the sample chamber was produced at the Leipniz Institute for Photonic Technologies (IPHT) Jena, FAG 53 microsystem technologies. The current wafer design followed previously optimized structures [17]. Here, a 100-mm round borofloat wafer with 1.1 mm thickness comprising 26 chips with 14.15 x 14.15 mm size was employed. Each numbered chip consisted of two photoresist coatings, i.e. a 1.1 µm thin layer for the cross-like trapping region and an 82 µm thick layer for the deep channels to the electrodes and the channels to the outer circle to compensate hydrodynamic flow. A color image of the wafer with PDMS on top is shown in Figure S7 A.

A PDMS mixture with a 1:10 ratio of polymer:hardener (Sylgard 184 elastomer, Dow Corning) was poured over the wafer in a petri dish and cured for 4 h at 70°C. The PDMS layer was carefully removed from the wafer, and each chip was cut out by a scalpel. Holes for the electrodes were punched using a sharpened needle. A single PDMS chip was sonicated in pure acetone, rinsed with deionized water and dried in a nitrogen stream. A 32 x 24 mm cover glass with defined thickness (#1.5) was rinsed with deionized water and dried in a nitrogen stream. PDMS and cover glass were evacuated for 15 to 20 min and were plasma-etched for 90 seconds. Because we studied time-dependent single-molecule enzyme kinetics, each sample chamber was prepared immediately before starting the measurements on the ABEL trap. Briefly, after PDMS was bonded to the cover glass, the sample chamber was filled quickly with 10 µl of the proteoliposome solution using a thin gel-loader tip, the sample chamber was clamped on the microscope, Pt-electrodes were put into the four holes, the laser focus pattern was positioned accurately in the center of the flat trapping region and the z-position of the focus was aligned. All procedures were completed within 2 minutes. Then smFRET data were recorded consecutively in five 5-min runs to limit the TCSPC file size. A color

image of the PDMS/glass sample chamber with electrodes clamped on top of the microscope is shown in Figure S7 B.

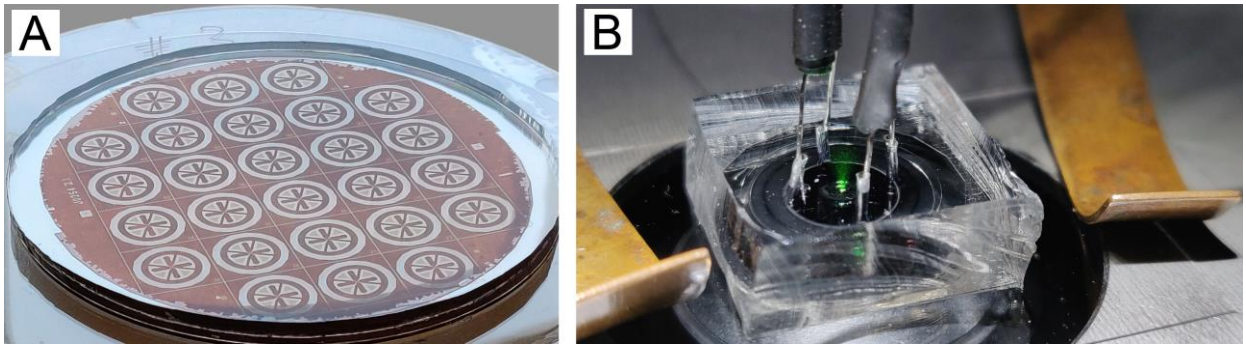

Figure S7. A, wafer with PDMS layer for 26 sample chambers. **B**, mounted ABEL trap chip with inserted electrodes and 532 nm laser on.

2.4. 32-point knight tour pattern. The focus pattern expanded the size of 532 nm excitation volume by a factor of ~5 as estimated from FCS measurements of Rhodamine 6 G (R6G) in aqueous solution (Figure S8 A). This was expected from the laser focus waist of 0.6 µm and given pattern dimensions of 2.34 x 2.34 µm. Due to the thin laser beam diameter < 1 mm underfilling the back aperture of the objective, the mean diffusion time of R6G was $\tau_{(D)}$ = 0.35 ms with the EODs turned off (black curve, FCS fitting shown as red curve). The FCS fitting model included a triplet term with $\tau_{(T)}$ = 3 µs. This diffusion time is indicated by the position of the black cross in Figure S8 A. Turning the knight pattern on altered the autocorrelation function G(τ) of R6G significantly (blue curve, FCS fitting shown as red solid line plus approximation to short correlation times as dotted red curve). The mean diffusion time shifted to $\tau_{(D)}$ = 1.67 ms (marked by the blue cross), and several strong correlations were visible. The 7 kHz repetition rate of the pattern corresponded to the peak at correlation time t=0.14 ms as marked by the blue asterisk. Additional faster correlations were revealed due to the 4.08 µs dwell for each point and a repeating overlap of the focus points within the knight pattern. Similarly the diffusion times of proteoliposomes in the cross-like shallow trapping region of the sample chip were extended, i.e. from $\tau_{(D)}$ = 35 ms with a single fixed laser position and inactive feedback (black curve in Figure S8 B) to $\tau_{(D)}$ ~ 270 ms with the knight tour pattern and the electrode feedback for trapping activated. Due to a repetition rate of 5 kHz, the related correlation peak was found at a correlation time of 0.2 ms (purple asterisk).

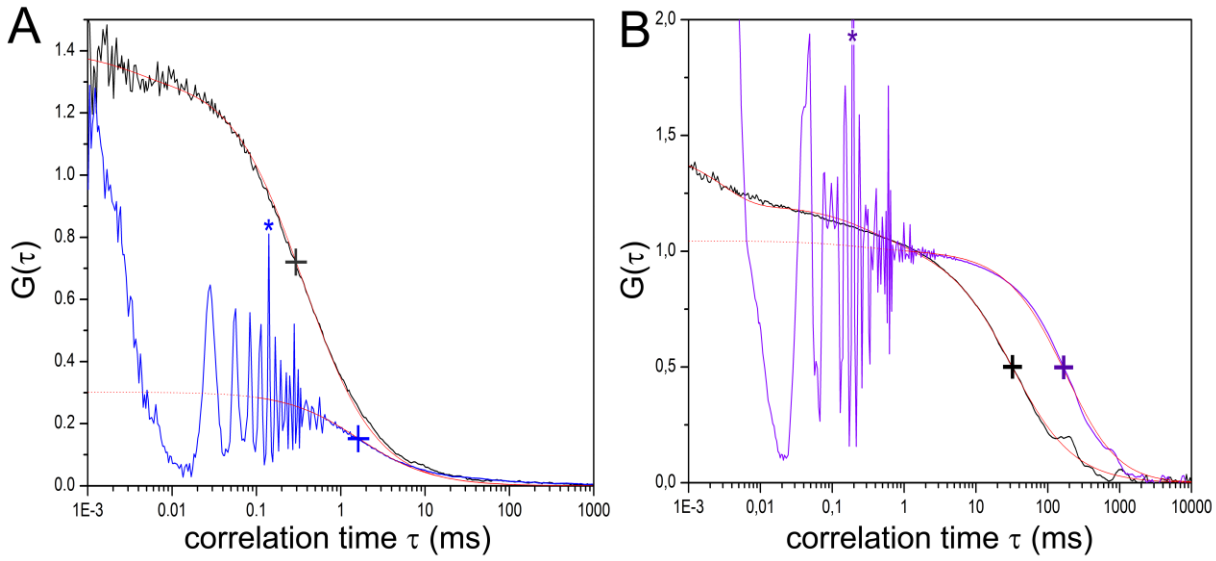

Figure S8. **A**, FCS of R6G in solution with 32-point knight tour pattern off (black curve) or with active pattern (blue curve). Blue asterisk denotes the correlation peak due to the 7 kHz repetition frequency of the pattern. Crosses indicate the mean diffusion times after fitting (red curves). **B**, normalized FCS of Cy3B-labeled F_oF_1 in liposomes with the 1 µm shallow region of the ABELtrap chip with 32-point knight tour pattern turned off (black curve) or pattern and electrode feedback active (purple curve). Purple asterisk denotes the correlation peak due to the 5 kHz pattern repetition frequency. Crosses indicate the mean diffusion times according to the fitting (red curves).

The corresponding fluorescence intensity time traces of these proteoliposomes recorded in the shallow trapping region are shown in Figure S9. Keeping the laser focus position fixed, freely diffusing single F_oF_1-ATP synthases yielded photon bursts with maximum peak counts around 150 counts per ms (or kHz, respectively), with the expected strong variations from burst to burst (Figure S9 A, black trace).

Turning the knight tour focus pattern on resulted in an estimated 5-fold drop of the peak intensities to around 30 kHz, with a few proteoliposomes exhibiting higher peak photon counts (due to aggregates of liposomes or reconstitution of more than one enzyme in a liposome). Obviously, the intensity drop was caused by expanding the excitation volume which reduced the mean excitation power per area, but also increased the observation time or diffusion time respectively (blue trace, Figure S9 B). A strong variability of the fluorescence peak intensities due to the arbitrary diffusive motion of the proteoliposomes through the focus remained for the expanded excitation volume. After starting the electrode feedback the duration and shape of the photon bursts changed (purple trace, Figure S9 C). The intensity variation within the burst and across bursts was much smaller, motion of the proteoliposomes through the focus remained for the expanded excitation volume.

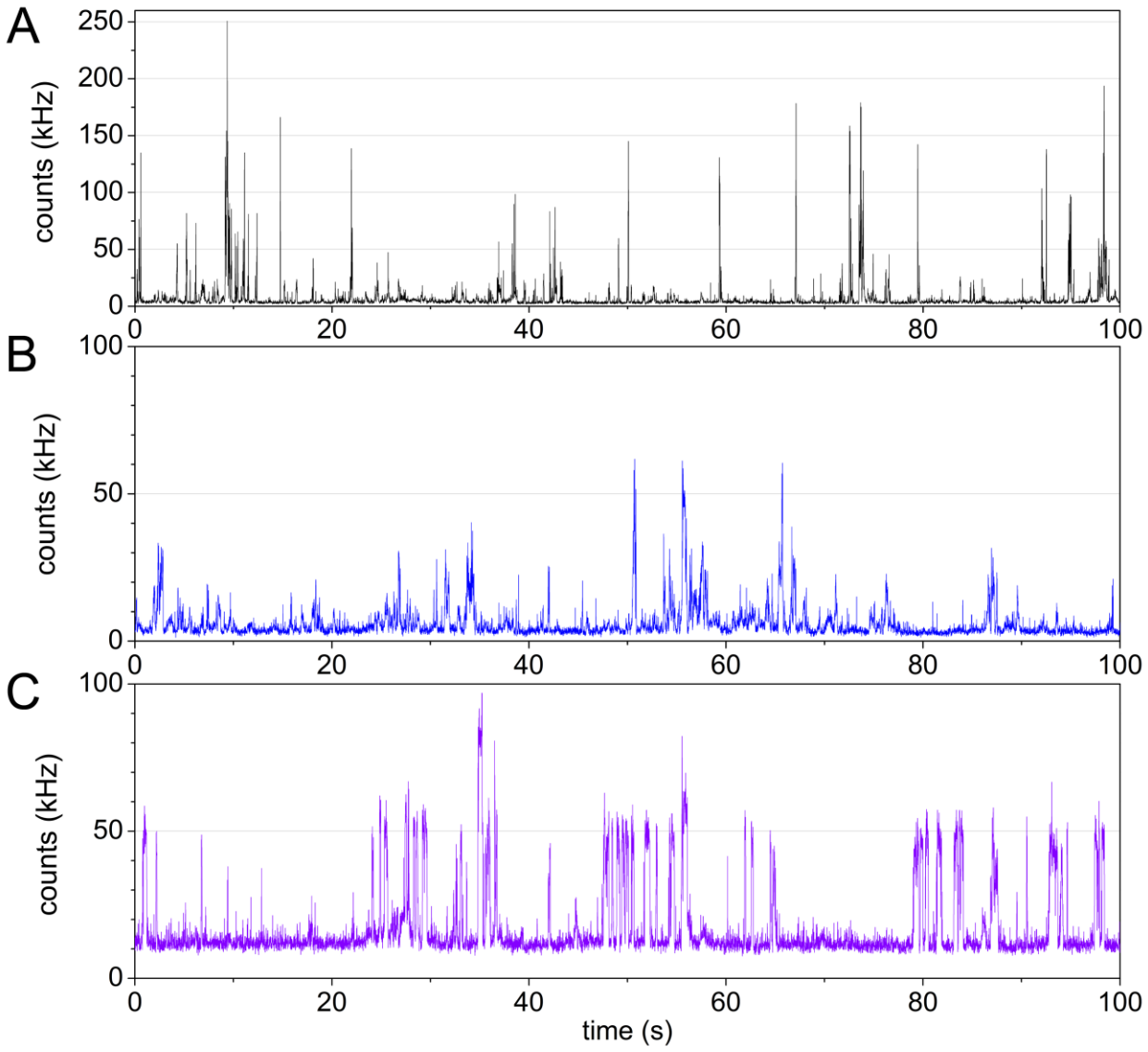

Figure S9. Fluorescence intensity time traces of FRET-labeled F_oF_1-ATP synthases in liposomes with 10 ms time binning, 532 nm excitation with 40 µW, intensities of FRET donor channel only. **A**, time trace with fixed laser focus position. **B**, time trace with 32-point knight tour focus pattern active. **C**, time trace with knight tour pattern and electrode feedback active, i.e. during ABEL trapping.

After starting the electrode feedback the duration and shape of the photon bursts changed (purple trace, Figure S9 C). The intensity variation within the burst and across bursts was much smaller, and the mean intensity level (~50 kHz) was higher than the average for freely diffusing proteoliposomes. However, also the background signal increased to ~10 kHz, resulting in a 4:1 signal-to-background ratio (note that this was the FRET donor channel only in Figure S9).

2.5. Photophysics of TMR, Cy3B and Atto R6G as FRET donor. To select an optimal FRET donor fluorophore for 532 nm excitation with the ABEL trap setup reconstituted F_oF_1-ATP synthases were labeled at residue εH56C with either tetramethylrhodamine (TMR), Cy3B or Atto Rho6G (or Atto R6G). At first, molecular brightness was estimated using spectral data for the fluorophores as provided by FPbase (open source website www.FPbase.org/spectra/). For the previously used fluorophore TMR for smFRET with F_oF_1-ATP synthase, the molar extinction coefficient at 532 nm was $\varepsilon_{(TMR,532)} = 53{,}000\ M^{-1}cm^{-1}$ (i.e. 53% of the maximum $\varepsilon_{(TMR,552)} = 100{,}000\ M^{-1}cm^{-1}$ at 552 nm), the fluorescence quantum yield was ϕ=0.34 and a relative spectral detection efficiency limited by the optical filter 582/75 BrightLine HC was 0.765. For Cy3B, the molar extinction coefficient at 532 nm was $\varepsilon_{(Cy3B,532)} = 78{,}000\ M^{-1}cm^{-1}$, ϕ=0.67 and the spectral detection efficiency 0.692. For Atto R6G, the molar extinction coefficient at 532 nm was $\varepsilon_{(Atto\ R6G,532)} = 115{,}000\ M^{-1}cm^{-1}$, ϕ=0.9 and the spectral detection efficiency 0.757. For comparison, the molecular brightness of Cy3B was calculated as the product of $\varepsilon_{(532)} * \phi *$ [spectral detection efficiency] and normalized to 100%. Accordingly, the expected relative molecular brightness for TMR was 38%, and for Atto R6G was 216%.

The experimental data in Figure S10 indicated that TMR attached to F_oF_1-ATP synthase exhibited a mean brightness of 14 kHz, Cy3B a mean of 34 kHz, and Atto R6G a mean of 41 kHz. The relative brightness of TMR was 41% with respect to Cy3B, and 121% for Atto R6G. A substantial asymmetry of the brightness distribution was noticed for Atto R6G attached to F_oF_1-ATP synthase (Figure S10 H).

Despite the different brightness of the three fluorophores, proteoliposomes were trapped with comparable probabilities. The burst duration distributions for TMR- or Atto R6G-labeled F_oF_1-ATP synthases were almost identical. Fitting the distributions with an exponential decay function yielded average trapping times of 350 ms for TMR and 370 ms for Atto R6G (1/e value), but Cy3B showed a significant longer average trapping time of 750 ms. Therefore, Cy3B was chosen as the FRET donor for smFRET measurements in the ABEL trap. Note that the mean count rates given in Figure S10 were smaller because only photons detected in the FRET donor channel were recorded. Therefore, using the total mean count rates in both FRET detection channel would have increased the mean count rates by 9% for TMR, by 16.5% for Cy3B and by 5.4% for Atto R6G.

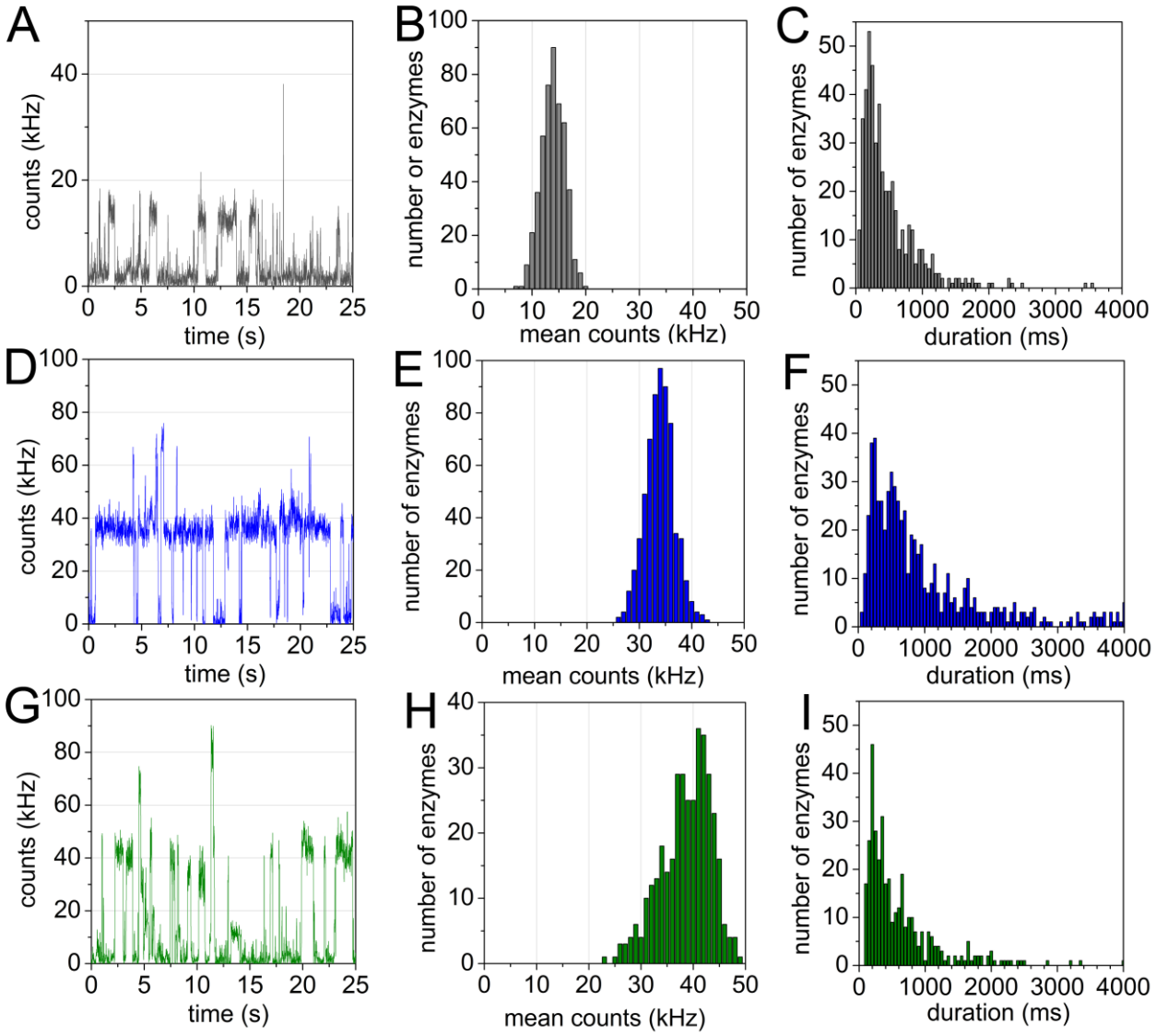

Figure S10. Comparison of TMR (grey), Cy3B (blue) and Atto R6G (green) attached to F_oF_1-ATP synthase in the ABEL trap. **A, D, G**, fluorescence intensity time traces with background subtracted, using 10 ms binning, recorded in the FRET donor channel**. B, E, H**, mean brightness distribution of ABEL trapped proteoliposomes. **C, F, I**, burst duration distribution of the ABEL trapped proteoliposomes.

3. Adding the antioxidant "*trolox*" as a triplet quencher

Photobleaching of the FRET acceptor Alexa Fluor was observed frequently for FRET-labeled F_oF_1-ATP synthases in the ABEL trap, affecting the high FRET state more severely than the medium FRET state as noticeable by fewer long-lasting high FRET photon bursts.

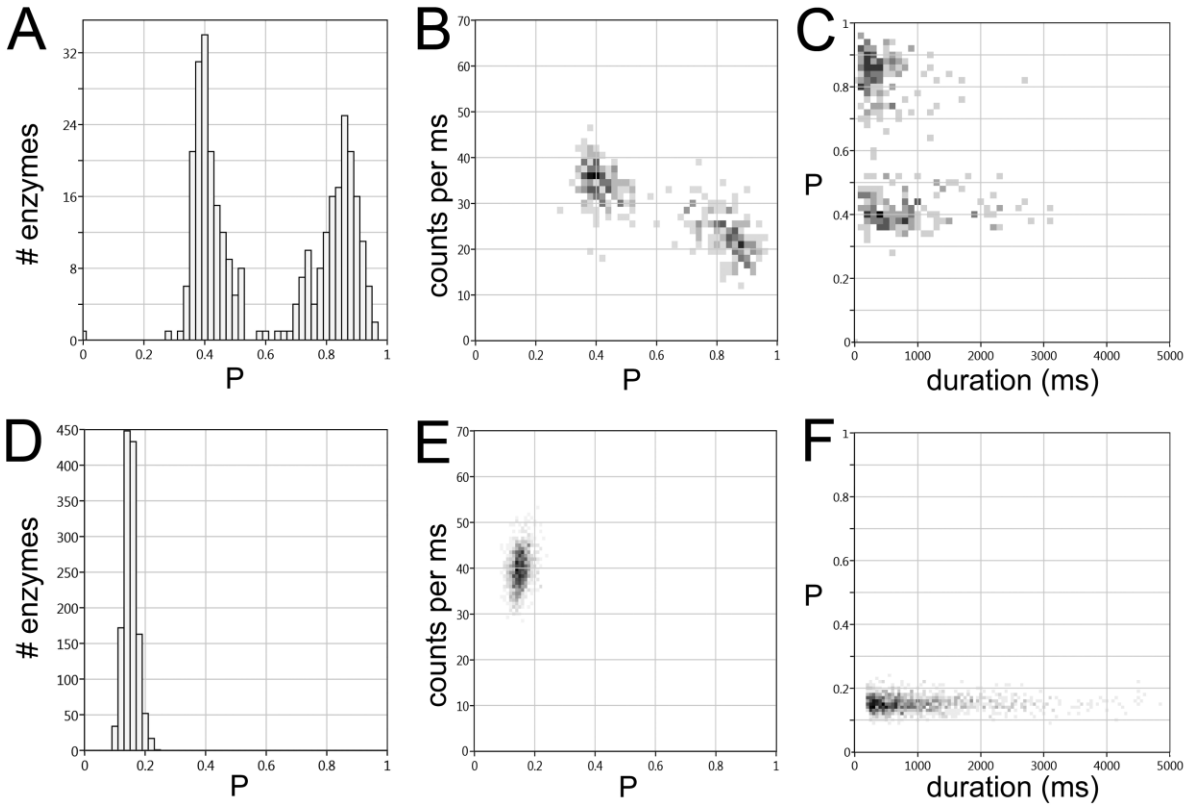

Figure S11. Proximity factor distributions, related brightness and burst durations of proteoliposomes in the presence of 1 mM AMPNPN and 2mM "*trolox*". **A, B, C**, FRET-labeled F_oF_1-ATP synthases with Cy3B attached to εH56C and Alexa Fluor 647 to a-CT. **D, E, F,** "donor only"-labeled F_oF_1-ATP synthases.

To extend the trapping duration and to reduce photobleaching of Alexa Fluor 647, the addition of 2 mM "*trolox*" to the proteoliposomes in the presence of 1 mM AMPPNP (or 1 mM ATP, respectively) was evaluated. As shown in Figure S11 in the presence of 1 mM AMPPNP, the two FRET subpopulations exhibited almost the same proximity factor distributions and P-related brightness as in the absence of "*trolox*". Also the medium FRET state subpopulation lasted slightly longer than the high FRET state subpopulation. Neither the mean brightness nor the trapping duration of "donor-only" enzymes with P ~0.15 did benefit from the addition of "*trolox*" so that adding this triplet quencher was not continued for the subsequent experiments on ATP-dependent kinetic catalysis of F_oF_1-ATP synthases.

4. Photon bursts at ATP concentrations of 100 µM, 40 µM, 20 µM, 5 µM

4.1. Photon bursts at 100 µM ATP. Two examples of FRET-labeled F_oF_1-ATP synthases exhibiting ATP hydrolysis-driven ε-subunit rotation in the presence of 100 µM ATP are shown in

Figure S12 A, B. Throughout the photon bursts, FRET donor (green trace) and FRET acceptor (red trace) intensities changed in an anticorrelated pattern. The mean catalytic rate was calculated by counting the number of proximity factor fluctuations (i.e. a pair of one medium FRET level at P~0.4 plus one high FRET level at P>0.8, blue trace in the upper subpanel) during the duration of FRET fluctuations within the photon burst. The enzyme in Figure 12 A had an average turnover of 146 ATP·s^{-1} as calculated from 74 full rotations in 1525 ms. The enzyme was recorded 22.7 min after start of the measurement (i.e. ~25 min after ATP addition). Apparently, this ABEL-trapped enzyme did not operate at constant speed. Three phases could be distinguished: at the beginning the turnover was slower with 82 ATP·s^{-1} for 220 (6 full rotations), followed by a fast catalytic phase with 185 ATP·s^{-1} for 975 ms (60 full rotations), and a slow phase for the remaining 330 ms with 73 ATP·s^{-1} (8 full rotations). The enzyme in Figure 12 B recorded 23.1 min after starting the ABEL trap measurement exhibited an average catalytic rate at 40 ATP·s^{-1} for 1365 ms. However, for the first 750 ms period the rate was only 12 ATP·s^{-1}, followed by a rate of 72 ATP·s^{-1} before the FRET acceptor photobleached.

4.2. Photon bursts at 40 µM ATP. Two examples of catalytically active FRET-labeled F_oF_1-ATP synthases in the presence of 40 µM ATP are shown in Figure S12 C, D. The enzyme in Figure 12 C was recorded 22.7 min after starting the ABEL trap measurement and exhibited an average catalytic rate of 138 ATP·s^{-1}. After a 1109 ms period of fast FRET fluctuations this F_oF_1-ATP synthase stopped turnover and remained in the medium FRET state (P~0.4) for 260 ms before the FRET acceptor photobleached and the enzyme was lost from the ABEL trap. The second example in Figure 12 D exhibited an average catalytic rate of 164 ATP·s-1 and was recorded 6.2 min after starting the ABEL trap measurement. During a first 230 ms period the rate was 225 ATP·s^{-1}, followed by a slower rate of 134 ATP·s^{-1}.

4.3. Photon bursts at 20 µM ATP. In Figure S12 E, two examples of catalytically active FRET-labeled F_oF_1-ATP synthases are shown back-to-back in the presence of 20 µM ATP. The first enzyme in the time trace exhibited an average catalytic rate of 29 ATP·s^{-1} during an 833 ms period. The two well-defined FRET level at P~0.4 and P~0.9 alternated with fast transitions (within 1 to 3 ms). After FRET acceptor photobleaching the "donor only"-labeled enzyme remained trapped for another 600 ms. The subsequent photon burst showed an enzyme comprising in ms, i.e. yielding an average catalytic rate of 78 ATP·s^{-1}. Both enzymes were observed 22 min after starting the ABEL traps recording. In Figure S12 F, the F_oF_1-ATP synthase was recorded after 1.7 min and was

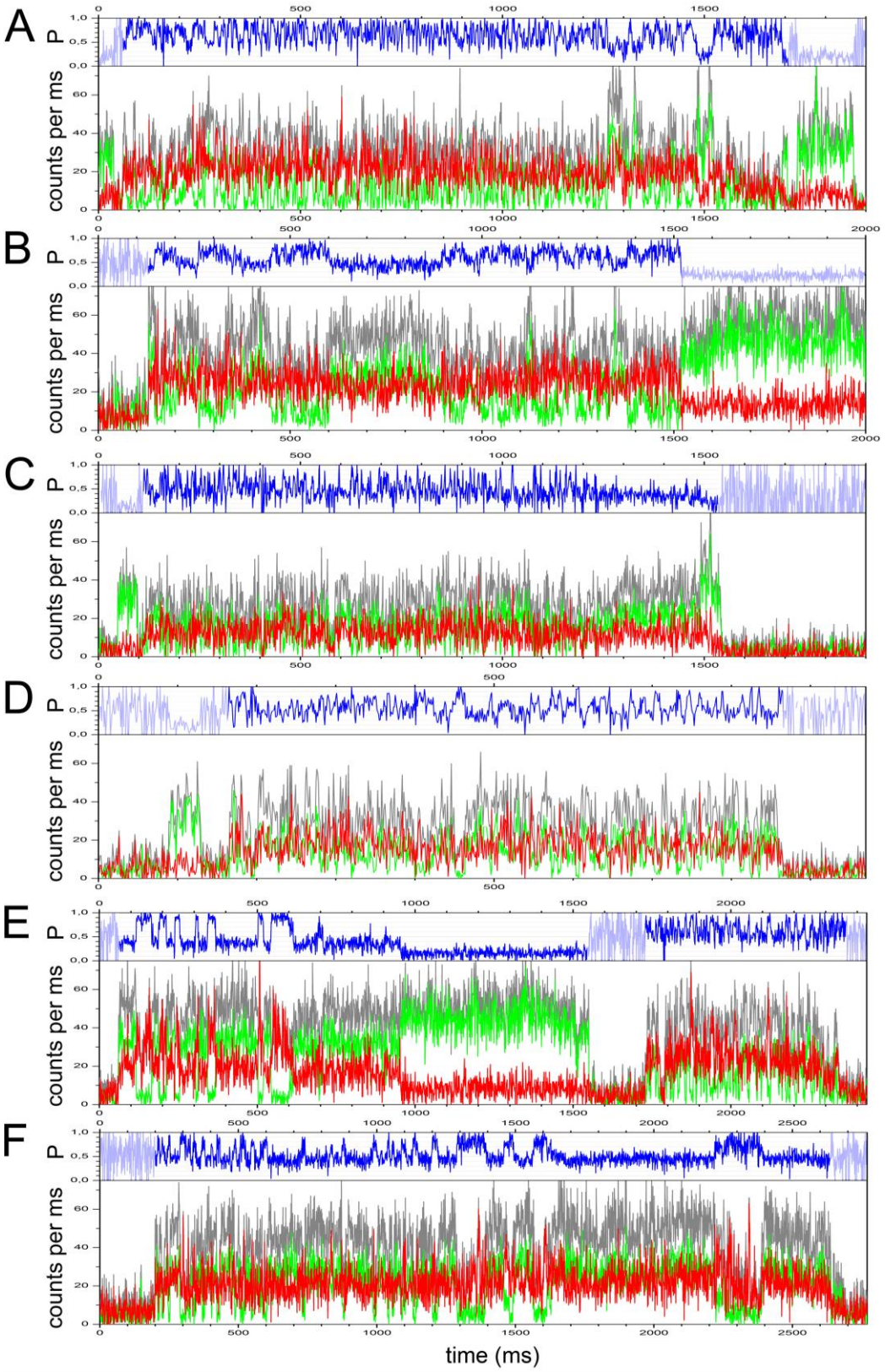

Figure S12. **A, B**, photon bursts of FRET-labeled F_oF_1-ATP synthases hold in the ABEL trap with 100 µM ATP. **C, D**, photon bursts with 40 µM ATP. **E, F**, photon bursts with 20 µM ATP. FRET donor intensity as green traces, FRET acceptor as red, summed intensities as grey, and proximity factor P in blue traces. 1 ms time binning.

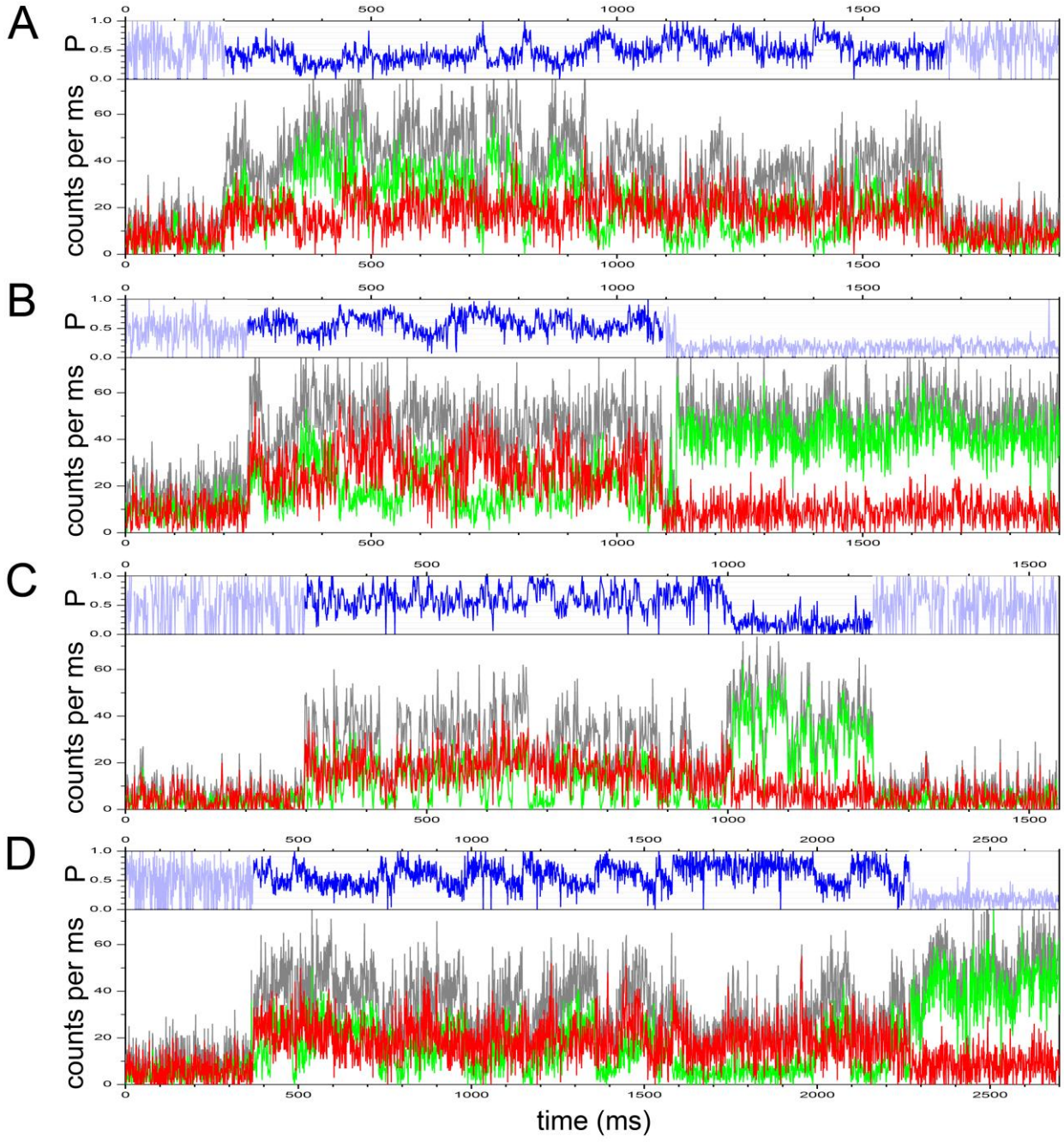

Figure S13. Photon bursts of FRET-labeled F_oF_1-ATP synthases in the presence of 5 µM ATP. FRET donor intensity as green traces, FRET acceptor as red traces, summed intensities as grey traces, and proximity factor P as blue traces. 1 ms time binning.

trapped for 2420 ms. The enzyme showed an average turnover of 29 ATP·s^{-1}. However, at the beginning the catalytic rate was faster with 97 ATP·s^{-1} or 13 full rotations in 404 ms, respectively. Then the catalytic rate dropped to 33 ATP·s^{-1} for 1080 ms, and slowed down even further. In the next 955 ms only three FRET level were found i.e. the enzyme almost stopped catalysis.

4.4. Photon bursts at 5 µM ATP. The lowest substrate concentration used in the experiments was 5 µM ATP. In Figure S13, four examples of active FRET-labeled F_oF_1-ATP synthases hold in solution be the ABEL trap are shown. In Figure S13 A, the enzyme recorded after 16.8 min, hydrolyzed ATP at an average rate of 19 ATP·s^{-1} during 950 ms. For the first ~500 ms of the photon burst the enzyme was found in the medium-to-low FRET state and was apparently inactive before starting ATP hydrolysis. In Figure S13 B, the enzyme had a turnover of 24 ATP·s^{-1} during 737 ms and was recorded 11.4 min after starting the ABEL trap measurement.

In contrast to fast FRET transition times of F_oF_1-ATP synthases in the presence of 20 µM ATP shown in Figure S12 E and F, switching between the medium FRET level at P~0.4 and P~0.85 occurred over several tens of ms and in an "ramp-like" behavior. In contrast, the enzyme in Figure S13 C exhibited fast FRET fluctuations yielding an average rate of 102 ATP·s^{-1} during 704 ms before FRET acceptor photobleaching. The fast catalysis of this enzyme was considered an outlier with respect to the mean ATP hydrolysis rate of 47 ATP·s^{-1} calculated from enzymes analyzed at 5 µM ATP. Another example of an active FRET-labeled F_oF_1-ATP synthase is shown in Figure S13 D. The ATP hydrolysis rate was 16 ATP·s^{-1} during 1844 ms before FRET acceptor photobleaching. FRET level transitions seemed to comprise not only P~0.4 and P> 0.8 but also an additional FRET level at 0.6<P<0.7 with a duration of 20 to 80 ms. Accordingly, an apparent FRET level sequence of →(P>0.8)→(P~0.65)→(P~0.4)→(P>0.8)→ could be assigned.

4.5. Duration of FRET fluctuations and related ATP hydrolysis rates. The durations of active catalysis of proteoliposomes in the ABEL trap were investigated for different ATP concentrations. For comparison, the distribution of "donor only" labeled F_oF_1-ATP synthases, had been fitted by a monoexponential decay and a 1/e trapping duration of 750 ms had been calculated. In the presence of different ATP concentrations, the distributions of FRET fluctuation periods for active enzymes appeared similar (Figure S14). Only a few enzymes were trapped for more than 1 second. Fitting the distribution in the presence of 1 mM ATP (Figure S14 A) yielded a 1/e duration of 350 ms for the mean catalytic activity, i.e. the distribution of the periods of catalytic activity were shorter than the trapping times of the "donor only" labeled F_oF_1-ATP synthases.

In the presence of 100 µM ATP and 50 µM CCCP, the durations of active catalysis were shorter than in the presence of the uncouplers valinomycin plus nigericin. (Figure S14 F, G). Because we noticed slightly different fluorescence or impurity background for each PDMS/glass chip and the

time-dependent bleaching of the background, these effects on the actual signal-to-background ratio might have caused different trapping behavior for some chips and might explain the apparent variations of the histograms of the active turnover periods.

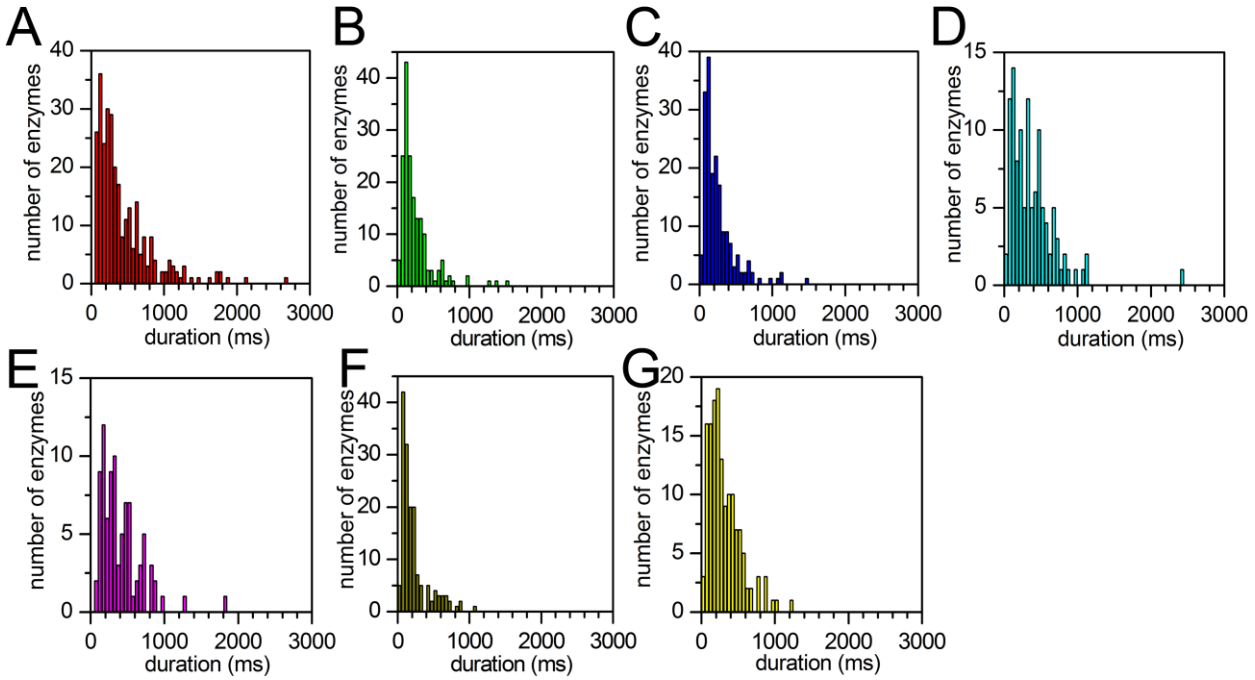

Figure S14. ATP-dependent distributions of FRET fluctuation periods from reconstituted F_oF_1-ATP synthases, in the presence of **A**, 1mM ATP, **B**, 100 µM ATP, **C**, 40 µM ATP, **D**, 20 µM ATP, **E**, 5 µM ATP, **F**, 100 µM ATP plus 50 mM CCCP, **G**, 100 µM ATP plus 1 µM valinomycin and 1 µM nigericin.

4.6. Analyzing ATP hydrolysis rates by Michaelis-Menten kinetics. The mean ATP hydrolysis rates obtained from the five ATP concentrations (1 mM, 100 µM, 40 µM, 20 µM and 5 µM) were used to estimate the maximum turnover speed $V_{(max)}$ and the Michaelis-Menten constant K_M.

Using the Lineweaver-Burk linearization [18] as shown in Figure S15, fitting (red line) resulted in $V_{(max)}$ = 147 ATP·s^{-1} from the intercept and K_M = 11,7 µM from the slope.

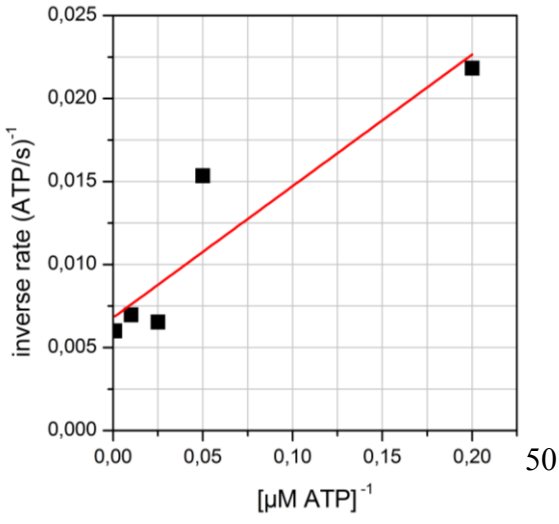

Figure S15. Lineweaver-Burk plot of ATP-dependent mean catalytic rates of FRET-labeled F_oF_1-ATP synthases hold in solution by the ABEL trap.

5. References for the Supporting Information

1. Borsch, M.; Diez, M.; Zimmermann, B.; Reuter, R.; Graber, P., Stepwise rotation of the gamma-subunit of EF(0)F(1)-ATP synthase observed by intramolecular single-molecule fluorescence resonance energy transfer. *FEBS letters* **2002,** *527* (1-3), 147-52.

2. Weiss, M.; Frohnmayer, J. P.; Benk, L. T.; Haller, B.; Janiesch, J. W.; Heitkamp, T.; Borsch, M.; Lira, R. B.; Dimova, R.; Lipowsky, R.; Bodenschatz, E.; Baret, J. C.; Vidakovic-Koch, T.; Sundmacher, K.; Platzman, I.; Spatz, J. P., Sequential bottom-up assembly of mechanically stabilized synthetic cells by microfluidics. *Nat Mater* **2018,** *17* (1), 89-96.

3. Zimmermann, B.; Diez, M.; Zarrabi, N.; Graber, P.; Borsch, M., Movements of the epsilon-subunit during catalysis and activation in single membrane-bound H(+)-ATP synthase. *The EMBO journal* **2005,** *24* (12), 2053-63.

4. Aggeler, R.; Capaldi, R. A., Cross-linking of the gamma subunit of the Escherichia coli ATPase (ECF1) via cysteines introduced by site-directed mutagenesis. *The Journal of biological chemistry* **1992,** *267* (30), 21355-9.

5. Aggeler, R.; Ogilvie, I.; Capaldi, R. A., Rotation of a gamma-epsilon subunit domain in the Escherichia coli F1F0-ATP synthase complex. The gamma-epsilon subunits are essentially randomly distributed relative to the alpha3beta3delta domain in the intact complex. *The Journal of biological chemistry* **1997,** *272* (31), 19621-4.

6. Heitkamp, T.; Deckers-Hebestreit, G.; Börsch, M., Observing single FoF1-ATP synthase at work using an improved fluorescent protein mNeonGreen as FRET donor. *Proc. SPIE* **2016,** *9714*, 97140B.

7. Wise, J. G., Site-directed mutagenesis of the conserved beta subunit tyrosine 331 of Escherichia coli ATP synthase yields catalytically active enzymes. *The Journal of biological chemistry* **1990,** *265* (18), 10403-9.

8. Duncan, T. M.; Duser, M. G.; Heitkamp, T.; McMillan, D. G.; Borsch, M., Regulatory conformational changes of the epsilon subunit in single FRET-labeled FoF1-ATP synthase. *Proc. SPIE* **2014,** *8948*, 89481J.

9. (a) Rosing, J.; Harris, D. A.; Kemp, A., Jr.; Slater, E. C., Nucleotide-binding properties of native and cold-treated mitochondrial ATPase. *Biochimica et biophysica acta* **1975,** *376* (1), 13-26; (b) Fischer, S.; Graber, P.; Turina, P., The activity of the ATP synthase from Escherichia coli is regulated by the transmembrane proton motive force. *The Journal of biological chemistry* **2000,** *275* (39), 30157-62.

10. (a) Lotscher, H. R.; deJong, C.; Capaldi, R. A., Interconversion of high and low adenosinetriphosphatase activity forms of Escherichia coli F1 by the detergent lauryldimethylamine oxide. *Biochemistry* **1984,** *23* (18), 4140-3; (b) Dunn, S. D.; Tozer, R. G.; Zadorozny, V. D., Activation of Escherichia coli F1-ATPase by lauryldimethylamine oxide and ethylene glycol: relationship of ATPase activity to the interaction of the epsilon and beta subunits. *Biochemistry* **1990,** *29* (18), 4335-40.

11. Fischer, S.; Graber, P., Comparison of ΔpH- and Δψ-driven ATP synthesis catalyzed by the H(+)-ATPases from Escherichia coli or chloroplasts reconstituted into liposomes. *FEBS letters* **1999,** *457* (3), 327-32.

12. Duser, M. G.; Bi, Y.; Zarrabi, N.; Dunn, S. D.; Borsch, M., The proton-translocating a subunit of F0F1-ATP synthase is allocated asymmetrically to the peripheral stalk. *The Journal of biological chemistry* **2008,** *283* (48), 33602-10.

13. (a) Zarrabi, N.; Clausen, C.; Duser, M. G.; Borsch, M., Manipulating freely diffusing single 20-nm particles in an Anti-Brownian Electrokinetic Trap (ABELtrap). *Proc. SPIE* **2013,** *8587*, 85870L; (b) Dienerowitz, M.; Heitkamp, T.; Gottschall, T.; Limpert, J.; Borsch, M., Confining Brownian motion of single nanoparticles in an ABELtrap. *Proc. SPIE* **2017,** *10120*, 1012017; (c) Dathe, A.; Heitkamp, T.; Pérez, I.; Sielaff, H.; Westphal, A.; Reuter, S.; Mrowka, R.; Börsch, M., Observing monomer - dimer transitions of neurotensin receptors 1 in single SMALPs by homoFRET and in an ABELtrap. *Proc. SPIE* **2019,** *10884*, 108840N.

14. Dienerowitz, M.; Howard, J. A. L.; Quinn, S. D.; Dienerowitz, F.; Leake, M. C., Single-molecule FRET dynamics of molecular motors in an ABEL trap. *Methods* **2021**.

15. Fields, A. P.; Cohen, A. E., Electrokinetic trapping at the one nanometer limit. *Proceedings of the National Academy of Sciences of the United States of America* **2011,** *108* (22), 8937-42.

16. Wang, Q.; Moerner, W. E., Optimal strategy for trapping single fluorescent molecules in solution using the ABEL trap. *Appl Phys B* **2010,** *99* (1-2), 23-30.

17. (a) Cohen, A. E.; Moerner, W. E., Method for trapping and manipulating nanoscale objects in solution. *Appl. Phys. Lett.* **2005,** *86*, 093109; (b) Rendler, T.; Renz, M.; Hammann, E.; Ernst, S.; Zarrabi, N.; Borsch, M., Monitoring single membrane protein dynamics in a liposome manipulated in solution by the ABELtrap. *Proc. SPIE* **2011,** *7902*, 79020M; (c) Su, B.; Duser, M. G.; Zarrabi, N.; Heitkamp, T.; Starke, I.; Borsch, M., Observing conformations of single FoF1-ATP synthases in a fast anti-Brownian electrokinetic trap. *Proc. SPIE* **2015,** *9329*, 93290A.

18. Lineweaver, H.; Burk, D., The Determination of Enzyme Dissociation Constants. *J. Am. Chem. Soc.* **1934,** *56* (3), 658–666.